SENSITIVITY EXPERIMENTS ON THE MONSOON ONSET TO DIFFERENTIAL HEATING

T.N. Krishnamurti

and

Y. Ramanathan

Department of Meteorology
Florida State University
Tallahassee, Florida 32306, U.S.A.

ABSTRACT

i) This paper examines some observational aspects of the evolution of energy exchanges and differential heating during the GARP Monsoon Experiment MONEX. The main findings are that

a) large increase in the kinetic energy of the total and the nondivergent component of the flows occurs over the Arabian Sea about a week prior to the onset of monsoon rains over central India.

b) The field of differential heating evolves during the onset period moving to a favourable position for the generation of eddy available potential energy and its release to eddy kinetic energy.

c) The release of eddy available potential energy goes to enhance the kinetic energy of the divergent circulations.

d) The kinetic energy of the divergent circulation does not increase much with time, this energy is shown to be transferred rapidly to the nondivergent motion via a number of interaction functions. The orientation of the divergent flows is shown to be of prime importance in these transfers during the onset, active, break and revival periods of the monsoons.

ii) Based on the above observational sequence of findings a series of numerical prediction experiments are constructed to examine the sensitivity of the monsoon onset to initially imposed fields of differential heating. The results of 96 hour integrations seem to confirm the large sensitivity of the evolution to the field of heating. The results of these integrations also show that the kinetic energy of the monsoon circulation increases via the rapid increase of interactions among the irrotational and the nondivergent modes.

1. INTRODUCTION

This paper is aimed towards providing some understanding of the link between the differential heating over land and ocean and the evolution of the monsoons. Fig. (1) illustrates the evolution of zonal kinetic energy of the 850 mb flows over the Arabian Sea during the GARP Summer Monsoon Experiment (MONEX). This diagram is based on an analysis of daily motion field, (Krishnamurti et al., 1981). An example of the analysis and the data sets is illustrated in Fig.(2).

The evolution of the summer monsoon is very well illustrated by the time history of the kinetic energy of low level flows. The kinetic energy shows an increase by an order of magnitude just prior to the onset of monsoon rains over India. The kinetic energy shows a rapid increase between the 11th and 17th June while the rains over central India commenced around the 18th June. In this paper we shall refer to June 11th as the date of the dynamical onset. After the 17th of June the level of kinetic energy remains at a higher level during June and July. This strong flow remains barotropically unstable (Krishnamurti et al.,1981) for long periods in the sense that (i) the meridional profile of the zonal flows satisfy the necessary conditions for the existence of barotropic instability; (ii) linear stability analysis shows that waves of the scale of the onset vortex and monsoon depression ($\approx$3000 km) have the largest growth rate; (iii) barotropic energy exchanges, evaluated from the data sets, show that the low level zonal flows steadily transfer energy to the eddies; and (iv) a simple barotropic prediction experiment initiated from a preonset vortex stage leads to its formation via essentially a conversion of the shear vorticity into the curvature vorticity.

A follow on study on the formation of the onset vortex (Ramanathan, 1981) was carried out with a multi-level primitive equation model. His study essentially confirms the barotropic evolution of this vortex.

An important question, not addressed by the aforementioned studies, relates to the zonal flow accelerations. Krishnamurti et al. (1981) pointed out that there are at least two major problems of interest during the onset of monsoons, one of these relates to the formation of the onset vortex but a much broader question is that of the response of the zonal flows to the field of differential heating, we shall examine this problem here. The study is divided into an observational part leading to a hypothesis for the construction of numerical experiments to study the zonal flow responses to imposed initial fields of differential heating.

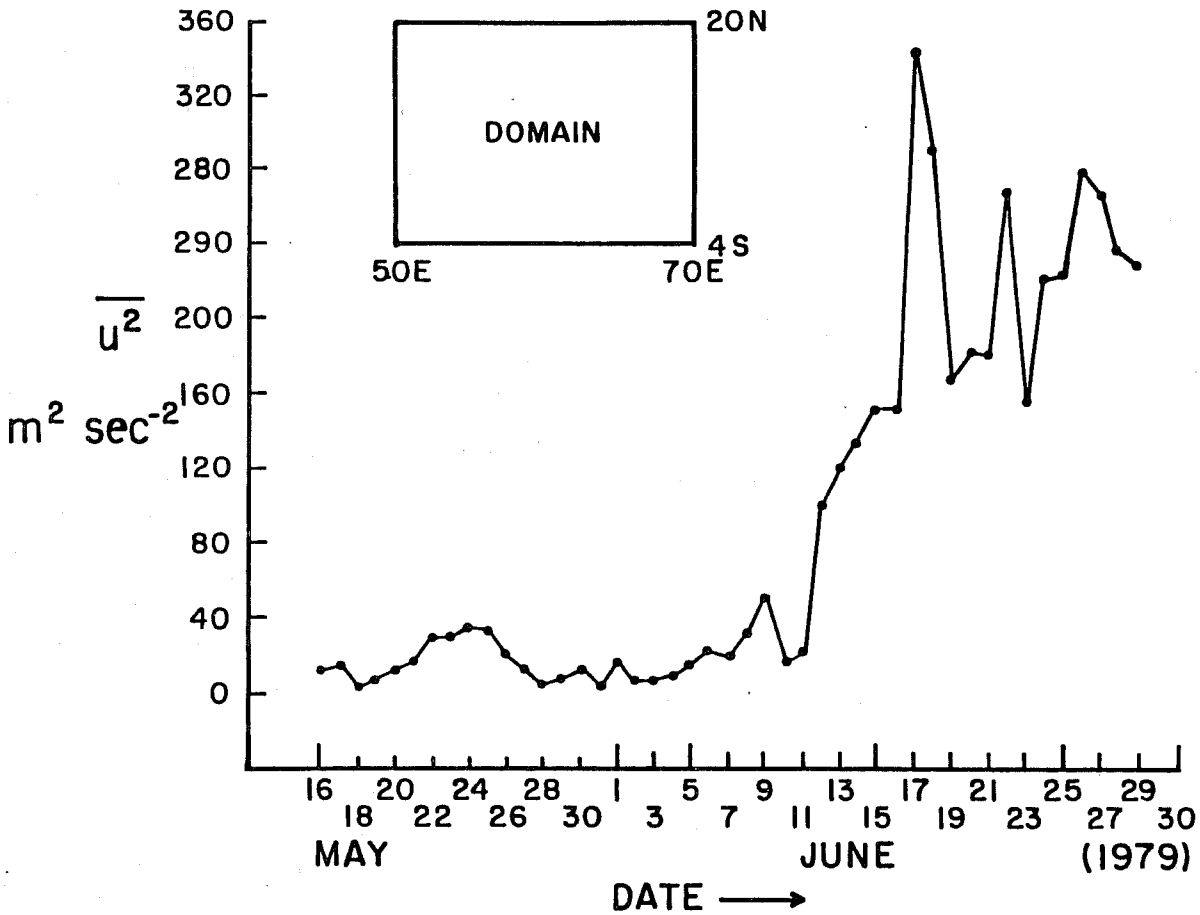

Fig. 1 A plot of domain averaged zonal kintic energy as a function of time over the Arabian sea. Units $m^2\ s^{-2}$.

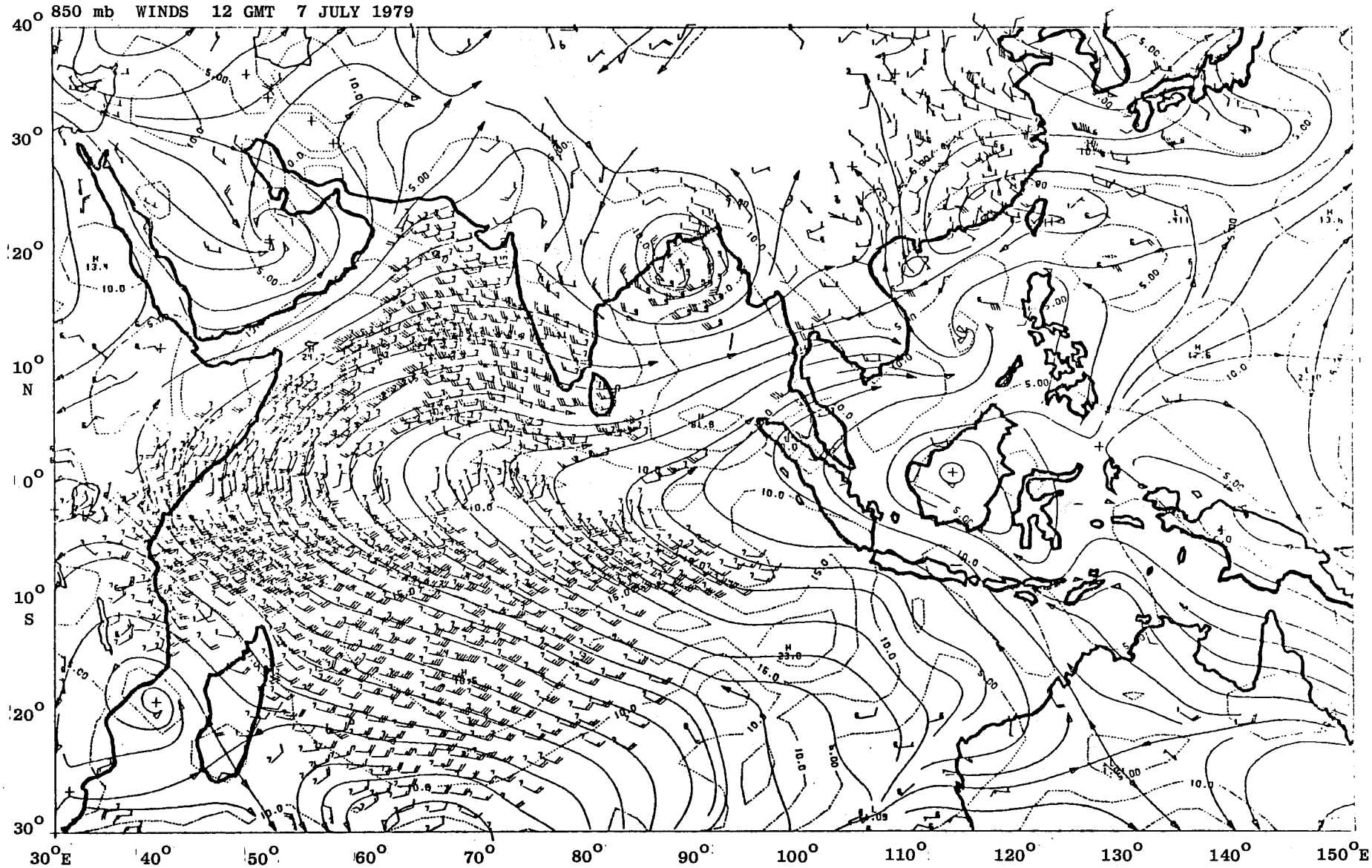

Fig. 2 A chart showing data coverage and analysis at 850 mb. Solid lines are streamlines, dashed lines isotachs m s^{-1}.

2. ON THE CALCULATION OF THE STREAMFUNCTION AND THE VELOCITY POTENTIAL

The approach we have followed is essentially that commonly used in spectral models (Daley et al., 1976). Here the u, v components of the velocity are expanded in a double Fourier representation along the zonal and meridional co-ordinates, with a truncation determined by the number of grid points in the zonal and meridional directions. The Fourier transform of these series yields expressions for the respective spectral coefficients U_i^m and V_i^m. Diagnostic relations exist similar to those proposed by Eliassen et al., (1970) that relate the spectral coefficients of divergence D_i^m and vorticity ζ_i^m to linear combinations of U_i^m and V_i^m. Similar relations can also be explicitly written down for the spectral coefficients of the streamfunction ψ_i^m and velocity potential χ_i^m such that, given U_i^m and V_i^m one can immediately obtain expressions for ζ_i^m, D_i^m, ψ_i^m and χ_i^m. The virtue of this scheme lies in that the sum of the irrotational and divergent motions yield the total wind field exactly. The disadvantage of this method lies in that it imposes a doubly periodic boundary condition in the zonal and meridional directions such that the fundamental mode is cyclic about the size of the computational domain. The latter appears to be not so serious if the computational domain is kept much larger than an area of interest. This is the case in the present study where the computational domain extends from 30^oE to 150^oE and 30^oS to 40^oN while the area of interest lies over the Arabian Sea, India and the Bay of Bengal and is much smaller.

3. PARTITIONING OF KINETIC ENERGY

The calculation of domain averaged kinetic energy of the nondivergent (ψ) and the irrotational (χ) motion fields during the evolution of MONEX is extremely revealing. Fig. (3 a,b,c) shows the time evolution of K_ψ and K_χ at the 850, 700 and 200 mb. A very sharp rise in K_ψ (from around 10 m^2s^{-2} to 70 m^2s^{-2}) is noted at the 850 mb level just prior to the onset, this is quite similar to the behaviour of the total kinetic energy illustrated earlier. The same sort of near exponential rise of irrotational kinetic energy (K_χ) is however not evident.

An increase of K_χ from around 5 m^2s^{-2} to around 10 m^2s^{-2} is noted after the 10th June, i.e. subsequent to the dynamical-onset over the Arabian sea. The evolution of the kinetic energy at 700 mb is quite similar to that at 850 mb. A period of decay of kinetic energy between July 10 and 20 coincides with a period of break in the monsoon rains. Around the period of the dynamical onset a sharp rise in the kinetic energy of the nondivergent flows is also noted at 200 mb, the ratio K_χ/K_ψ is largest at 200 mb being around 1/3, while it is around 1/8 at 700 mb and 1/7 at 850 mb. It is quite clear that at all these levels there are essentially two dynamical regimes of circulations (i) that prior to the 10th of June and (ii) that subsequent to the 10th June. The evolution of the total kinetic energy at the

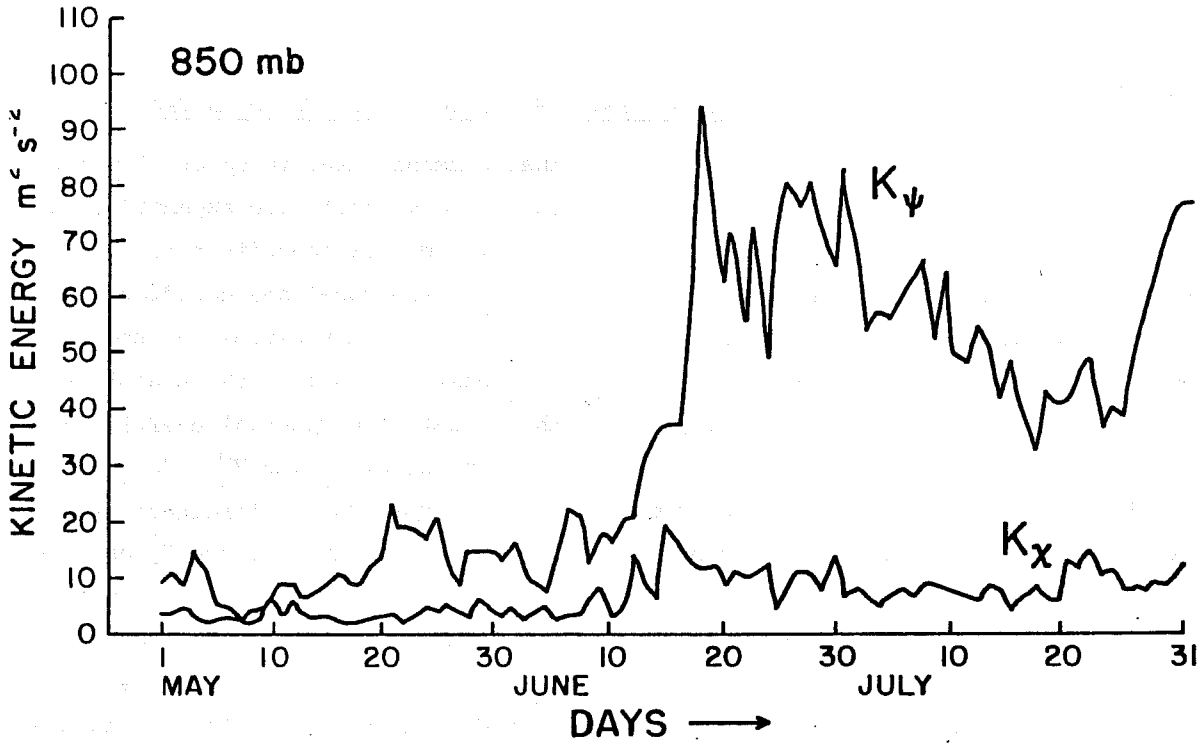

Fig. 3a The time variation of the kinetic energy of the irrotational component K_χ and the nondivergent component K_ψ. Units $m^2\ s^{-2}$. For 800 mb.

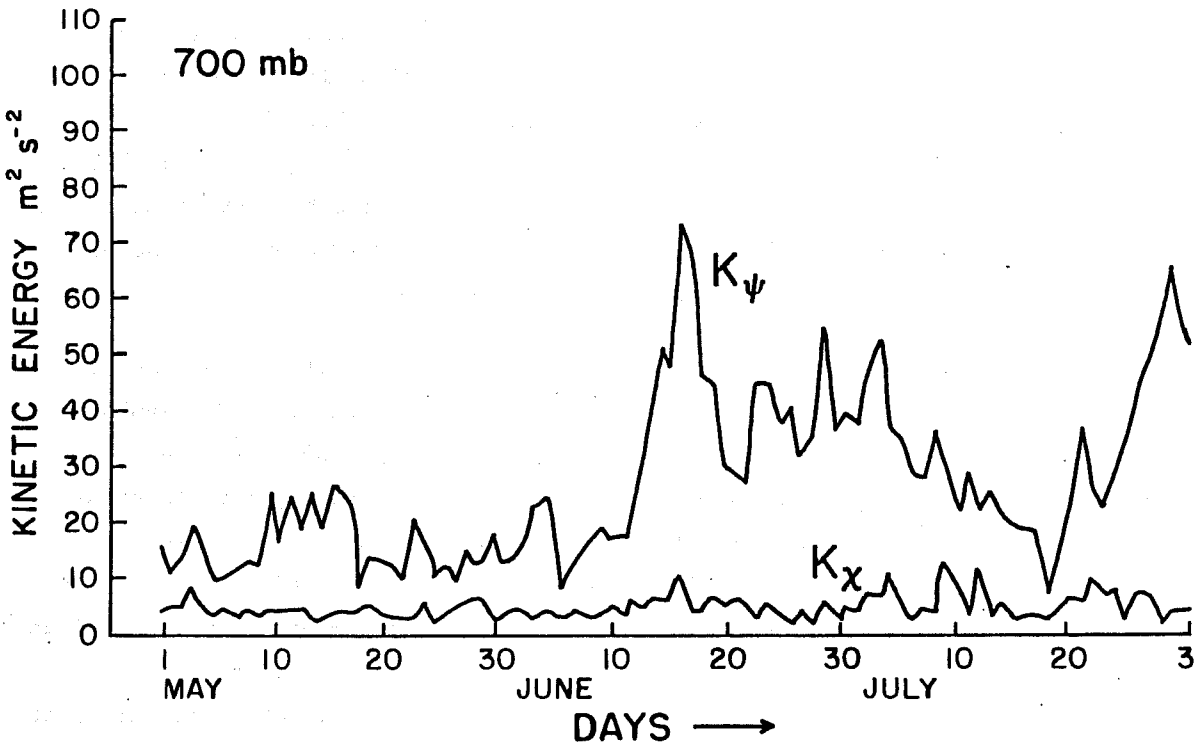

Fig. 3b As Fig. 3a but for 700 mb.

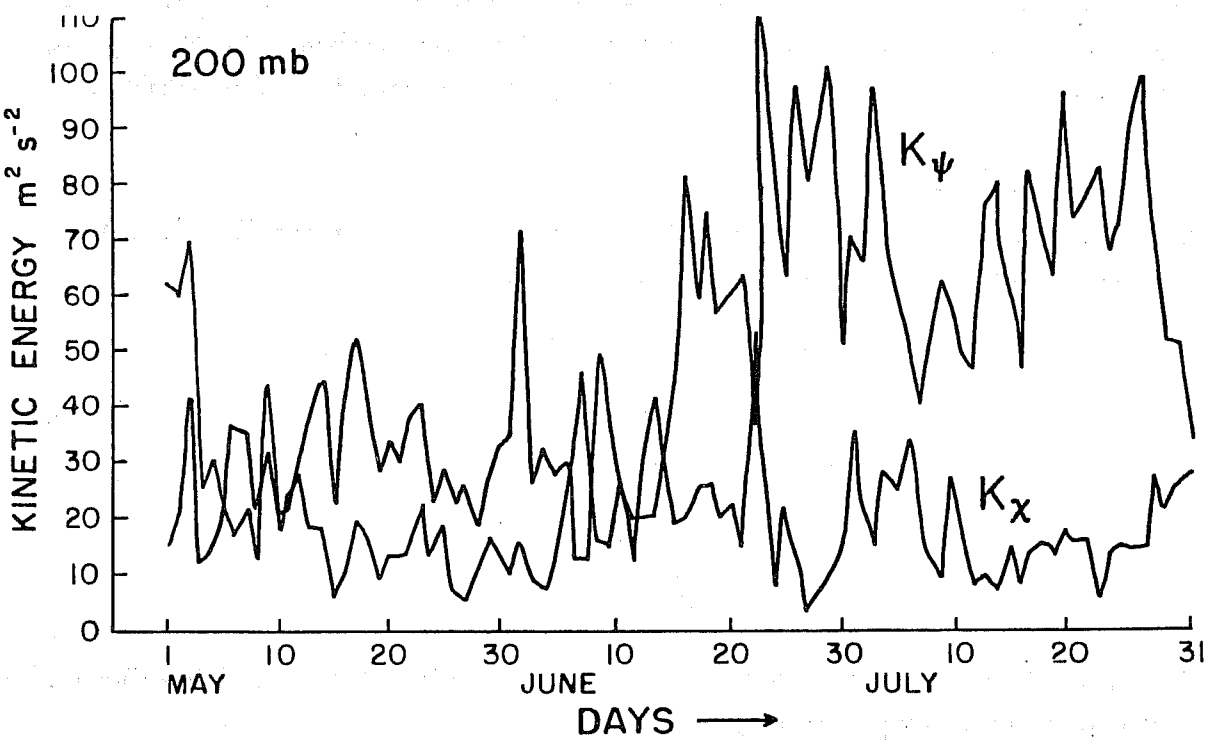

Fig. 3c As Fig. 3a but for 200 mb.

three levels is quite similar to that of the nondivergent component. The behaviour of the irrotational component is interesting from the standpoint of the overall monsoon dynamics. Energy transformation equations show that all of the available potential energy released via vertical circulations (east-west or Hadley type) must go to the irrotational component. Since the level of the energy of irrotational component remains nearly invariant during the entire period while the Hadley and east-west circulations prevail, the energy received by the irrotational component must be quickly passed on to the nondivergent component to build up K_ψ. This would occur via $\langle\psi.\chi\rangle$ interactions, we present in the following section.

4. ψ-χ INTERACTIONS

The conventional breakdown of the horizontal wind $\mathbf{V}_H$ into irrotational and non-divergent components may be expressed by the relations

$$\mathbf{V}_H = \mathbf{V}_\psi + \mathbf{V}_\chi \qquad 1\ (a)$$

$$\mathbf{V}_\psi = \mathbf{k} \times \nabla\psi \qquad 1\ (b)$$

$$\mathbf{V}_\chi = -\nabla\chi \qquad 1\ (c)$$

$$\nabla \cdot \mathbf{V}_H = -\nabla^2\chi \qquad 1\ (d)$$

and

$$\mathbf{k} \cdot \nabla \times \mathbf{V}_H = \nabla^2\psi$$

Here ψ is the streamfunction and χ is the velocity potential. The energy equations in terms of these components may be expressed by,

$$\frac{\partial}{\partial t} K_\psi = \nabla\cdot\psi\nabla\frac{\partial\psi}{\partial t} + \psi\nabla\cdot f\nabla\chi + \psi\nabla\chi\cdot\nabla(\nabla^2\psi) + \psi\nabla^2\chi\nabla^2\psi + \psi\omega\frac{\partial}{\partial p}\nabla^2\psi + \psi\nabla\omega\cdot\nabla\frac{\partial\psi}{\partial p} + \psi J\left(\omega, \frac{\partial\chi}{\partial p}\right) + \psi J(\psi, \nabla^2\psi + f) + F_\psi \qquad (2)$$

$$\frac{\partial}{\partial t} K_\chi = \nabla\cdot\chi\nabla\frac{\partial\chi}{\partial t} - \chi\nabla^2\phi + \chi\nabla\cdot f\nabla\psi + \chi(\nabla^2\psi)^2 - \chi\nabla^2\frac{(\nabla\psi)^2}{2} - \chi\nabla^2\frac{(\nabla\chi)^2}{2} - \chi\nabla\psi\cdot\nabla(\nabla^2\psi) + \chi\omega\frac{\partial}{\partial p}\nabla^2\chi + \chi\nabla\omega\cdot\frac{\nabla\partial\chi}{\partial p} + \chi J\left(\omega, \frac{\partial\psi}{\partial p}\right) + \chi\nabla^2 J(\psi,\chi) + \quad + \chi J(f,\chi) - \cdot - \chi J(\chi, \nabla^2\psi) + F_\chi \qquad (3)$$

Upon integration of the above equations over a horizontal domain and some re-arrangement of terms we can express the energy equation for the non-divergent and irrotational components by the relations,

$$\frac{\partial}{\partial t}\overline{\overline{K_\psi}} = B_\psi + \overline{\overline{f\nabla\psi\cdot\nabla\chi}} + \overline{\overline{\nabla^2\psi\nabla\psi\cdot\nabla\chi}} + \overline{\overline{\nabla^2\chi\,\frac{(\nabla\psi)^2}{2}}} + \overline{\overline{\omega J\left(\psi,\frac{\partial\chi}{\partial p}\right)}} + F_\psi \qquad (4)$$

$$\frac{\partial}{\partial t}\overline{\overline{K_\chi}} = B_\chi - \overline{\overline{\chi\nabla^2\phi}} - \overline{\overline{f\nabla\ \psi\cdot\nabla\chi}} - \overline{\overline{\nabla^2\psi\nabla\psi\cdot\nabla\chi}} - \overline{\overline{\nabla^2\chi\,\frac{(\nabla\psi)^2}{2}}} - \overline{\overline{\omega J\left(\omega,\frac{\partial\chi}{\partial p}\right)}} + F_\chi \qquad (5)$$

Here B_ψ and B_χ denote boundary fluxes and terms expressed by double overbar $\overline{\overline{\ \ }}$ denote the $\langle\psi\cdot\chi\rangle$ interactions. An equation for the time rate of change of internal plus potential energy over a closed domain may be expressed by a similar relation.

For a closed system (B=0), in the absence of heating and friction the sum of internal, potential plus kinetic energies of irrotational and nondivergent motion vanishes. The role of differential heating is in its net generation of internal plus potential energy via the heating of relatively warmer air and cooling of relatively cooler air, i.e. $H'T' > 0$.

If this does not occur, then the role of differential heating is dynamically passive. This generation of internal plus potential energy is usually accompanied by an ascent of warmer air and a descent of colder air. This process transforms (the generated) internal plus potential energy into the irrotational kinetic energy. The interaction is the only means available for the non-divergent motion to receive kinetic energy from the irrotational motions over a closed domain. Thus we envisage an involved energy transfer process from the differential heating to the eventual strong non-divergent motions of the monsoons.

We shall next examine the $\langle\psi\cdot\chi\rangle$ interactions. The magnitudes of term $\langle f\nabla\psi\cdot\nabla\chi\rangle$ depends on the orientation of the vectors $\nabla\psi$ and $\nabla\chi$. If over the northern hemisphere they are parallel, i.e., $\nabla\psi\cdot\nabla\chi > 0$, then energy exchanges go from the irrotational to the non-divergent modes. A similar argument holds for the second term $\langle\nabla^2\psi\nabla\psi\cdot\nabla\chi\rangle$ over regions of cyclonic vorticity over the northern hemisphere. The converse is the case over the southern hemisphere. The converse argument also holds for anti-parallel vectors, i.e. $\nabla_\psi\cdot\nabla\chi < 0$. The third term in this sequence $\langle\nabla^2\chi\ \nabla\psi\cdot\nabla\psi/2\rangle$ expresses another kind of $\langle\psi\cdot\chi\rangle$ interaction where the covariance of the horizontal divergence and the kinetic energy of the non-divergent component is important. At a similar point the contribution of this term alone has the form, $\partial/\partial t\ (\nabla\psi\cdot\nabla\psi/2) = \nabla^2\chi\cdot\nabla\psi\cdot\nabla\psi/2$ and leads to an exponential growth of the non-divergent

kinetic energy wherever the horizontal divergence ($\nabla^2\chi > 0$) is positive. The last term in this sequence, i.e., $\langle\omega J(\psi,\partial\chi/\partial p)\rangle$ defies a simple interpretation. Regions of large $\partial\chi/\partial p$ are generally also associated with regions of large vertical variations of convergence, i.e. $\partial\chi/\partial p \approx -\lambda^2\, \partial/\partial p\, \nabla^2\chi$. Following the streamfunctions, downstream from these regions energy exchange from irrotational to the non-divergent flows can occur if there is general upward motion. The converse being the case upstream of these regions. Order of magnitude calculations shows that the leading term among these are the first two that depend on the orientation of $\nabla\psi$ and $\nabla\chi$. Furthermore, it turns out that the geometry of low level monsoonal flows is anti-cyclonic just north of the equator, i.e., $\nabla^2\psi < 0$ whereas $f > 0$ thus the first two terms oppose each other, however $f\nabla\psi\cdot\nabla\chi$ is the largest term.

The determination of a complete observational energy budget is not the objective of the present study. The observational part of this work will focus on the time variability of a number of components during the entire period of the summer monsoons. We feel that much can be learned by this approach without resorting to the construction of a matched budget.

5. OBSERVATIONAL RESULTS OF ψ-χ INTERACTIONS

Throughout this paper the energy parameters and their exchanges are calculated over a domain 50°E to 100°E, 10°S to 20°N. The raw data, u, v analysis and the ψ, χ fields however were obtained over a bigger domain extending from 30°E to 150°E, 30°S to 40°N. Here we shall illustrate the time history of the four leading terms of the ψ-χ interactions. All the calculations are shown at 850 mb where the data sets are most complete (Fig. 2). The four leading terms require estimates of ψ, χ, $(\partial\chi/\partial p)$ and ω at 850 mb. ω is determined from the mass continuity equation by assuming zero vertical motion at 1000 mb. $(\partial\chi/\partial p)$ was obtained from the data sets at 850 and 700 mb via a one sided difference. Fig. 4 shows domain averages of these terms.

i) $\overline{f\nabla\psi\cdot\nabla\chi}$: This term depends on the orientation of $\nabla\psi$ and $\nabla\chi$ and turned out to be the leading one among the interaction terms. Its magnitude during May 1979 was around 50×10^{-6} m^2 s^{-3}, thereafter it exhibited a very rapid increase to around 400×10^{-6} units. The period of rapid increase precedes the dynamical onset by about a week and by about 2 to 3 weeks the onset of rains over Central India. A period of decrease of this interaction during July coincides with a period of Breaks in the Monsoons over India. The sharp changes in this interaction should be easy to see on charts of ψ, χ and $f\,\nabla\psi\cdot\nabla\chi$ during different epochs of the monsoons. Figs. (5 a,b,c,d,e and f) illustrate these fields for selected periods during the course of the

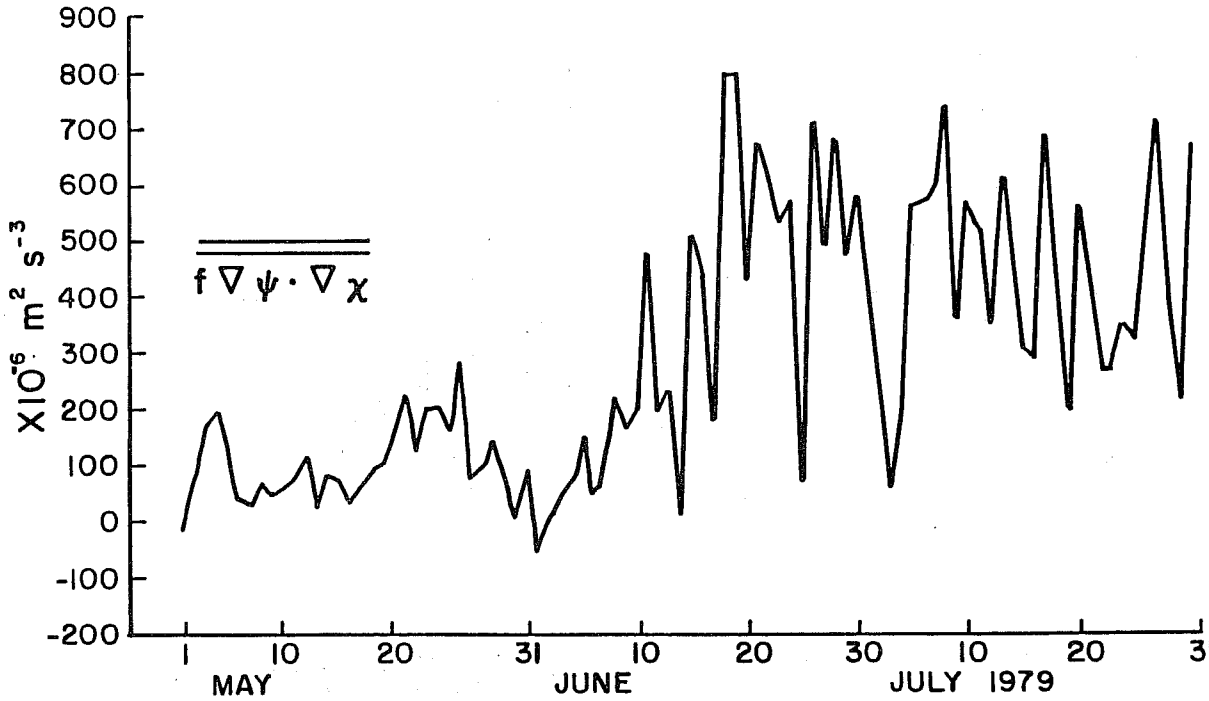

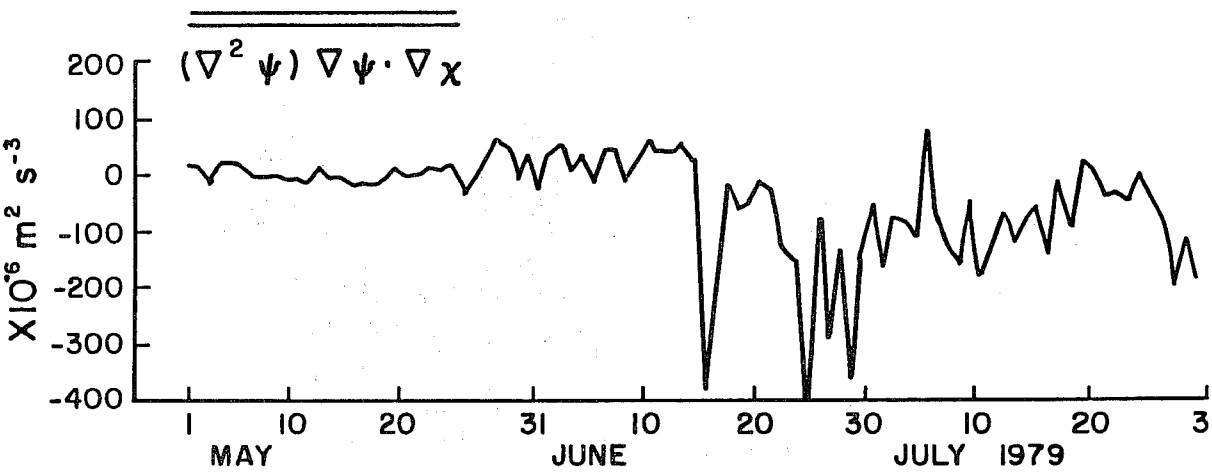

Fig. 4 a (top) b (bottom). Time variation of the different terms of the $\langle \psi . \chi \rangle$ interactions averaged over a domain. Units $10^{-6} m^2 s^{-3}$.

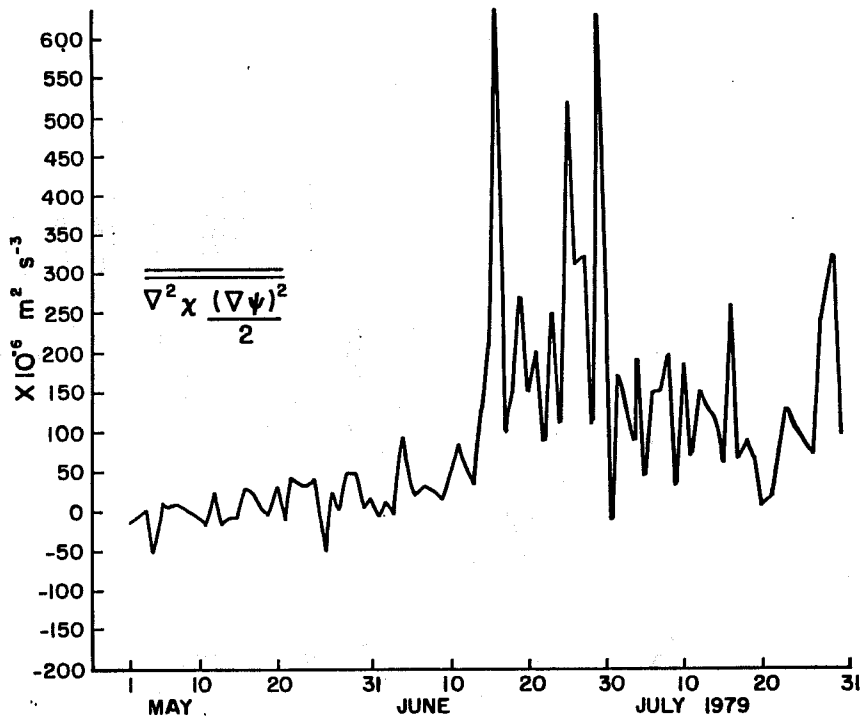

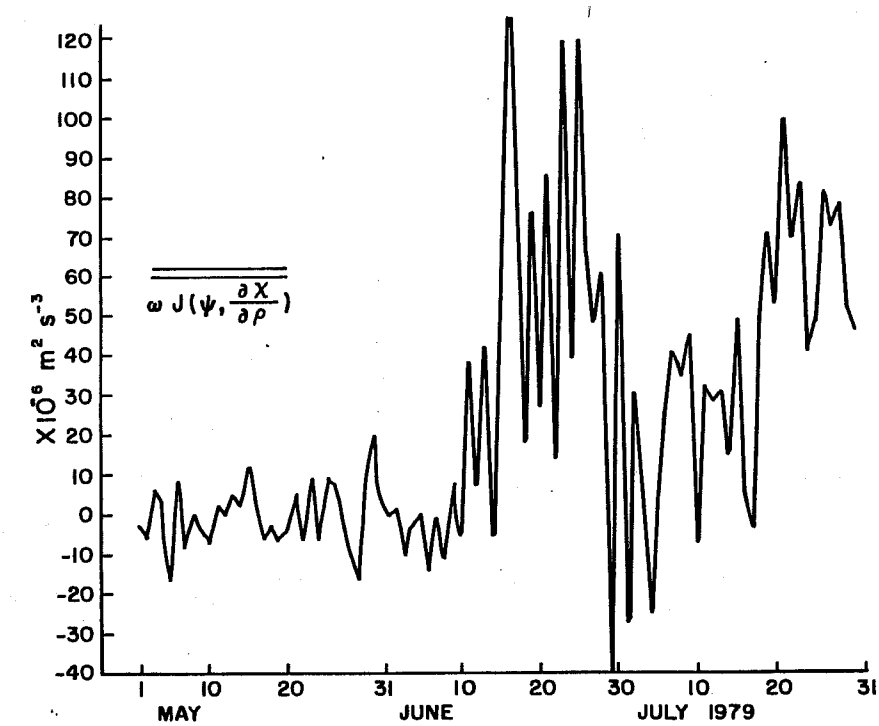

Fig. 4 c (top) d (bottom). As for Fig. 4a,b.

evolution of monsoons for 1979. These denote the following periods:

(a) May 2 - 6 1979, late spring

(b) June 1 - 5 1979, preonset

(c) June 12 - 16 1979, onset

(d) June 26 - 30 1979, active monsoons

(e) July 3 - 7 1979 monsoon depression

(f) July 11 - 15 1979, break monsoons

(g) 2nd half of July, revival of monsoons

The regions over the Arabian Sea, Bay of Bengal and the southern Indian Ocean (trade wind belt) exhibit the most interesting evolutions in the orientation of the $\nabla\psi$, $\nabla\chi$ vectors.

Northern Arabian Sea encountered strong winds (V_H most of which is V_ψ) after the 10th June. f $\nabla\psi\cdot\nabla\chi$ is extremely weak over this region for the late spring and preonset periods. The onset period shows an interesting orientation of $\nabla\psi$ and $\nabla\chi$. In this region both $\nabla\psi$ and $\nabla\chi$ acquire an equatorward orientation and sharp rise in the energy exchange from the irrotational to the non-divergent component occurs. When one examines the orientation during the Active, depression and Break periods the impression one gets is that $\nabla\psi$ does not change its orientation as much as $\nabla\chi$ does. The active and depression periods seem to coincide with nearly zonal orientations for the ψ and χ isopleths; the preonset and the break periods are characterised by a zonal orientation for the ψ isopleth while a more meridional (northwest to southeast) orientation for the χ isopleths. The χ isopleths undergo very interesting fluctuations in their orientation - this is obviously related to the manner in which they extract energy from the differential heating via vertical overturnings and pass it on to the nondivergent modes without substantially altering their own energy K_χ.

An important sidelight of the present study was on the dynamics of the trade wind belt. Throughout the period of this study, the orientation of $\nabla\psi$ and $\nabla\chi$ was very favourable for the transfer of energy from the irrotational to the non-divergent modes. This is apparent in these diagrams; i.e. f < 0, $\nabla\psi\cdot\nabla\chi < 0$, f $\nabla\psi\cdot\nabla\psi > 0$. This region over the southern Indian Ocean experiences strongest descent around 25^{o}S, the trade wind belt lies just north of this region, here the magnitude of $\nabla\chi$ is quite large and a steady transfer of energy goes on nearly all the time. This energy must be lost by dissipation in the boundary layer by the nondivergent motions whose intensity does not continually build up with time. In this region the descending branch of the monsoonal Hadley cell provides the energy for the irrotational motions while the $\psi \cdot \chi$ interactions play a key role in the maintenance of the trades.

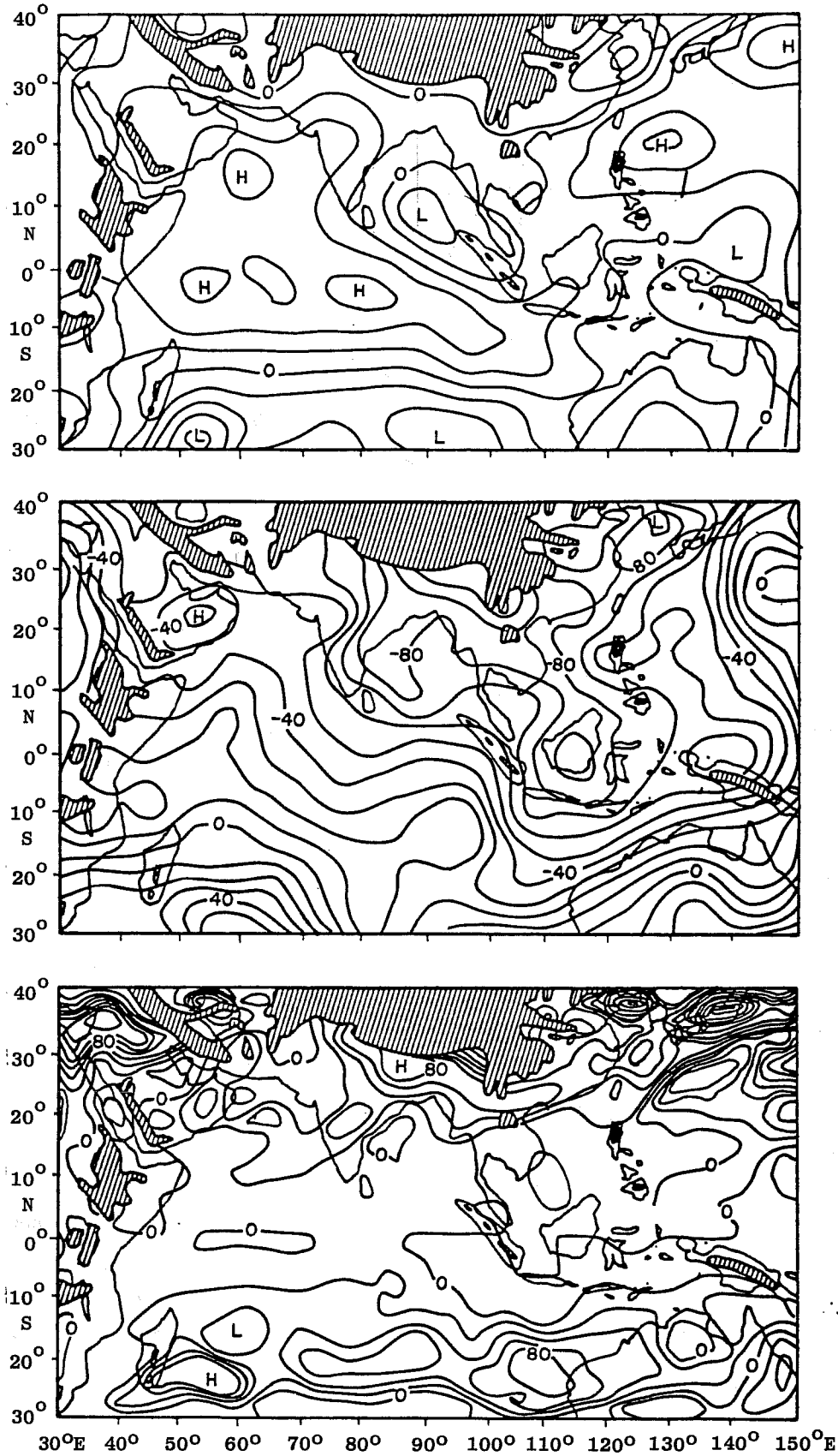

Fig. 5a Charts of the streamfunction ψ, velocity potential χ and of $f\nabla\psi.\nabla\chi$ for selected period during MONEX for late spring.

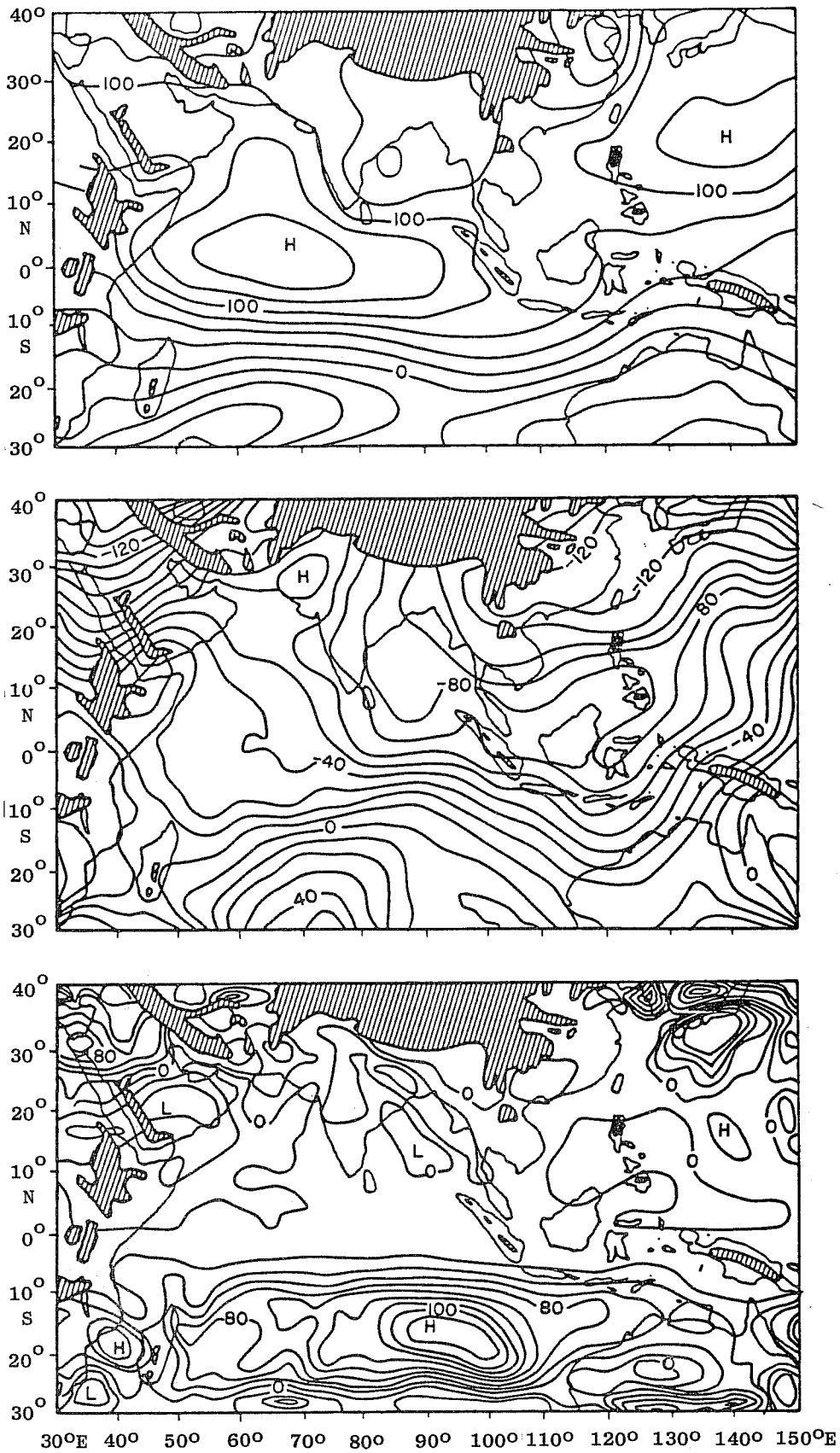

Fig. 5b As Fig. 5a but for pre-onset.

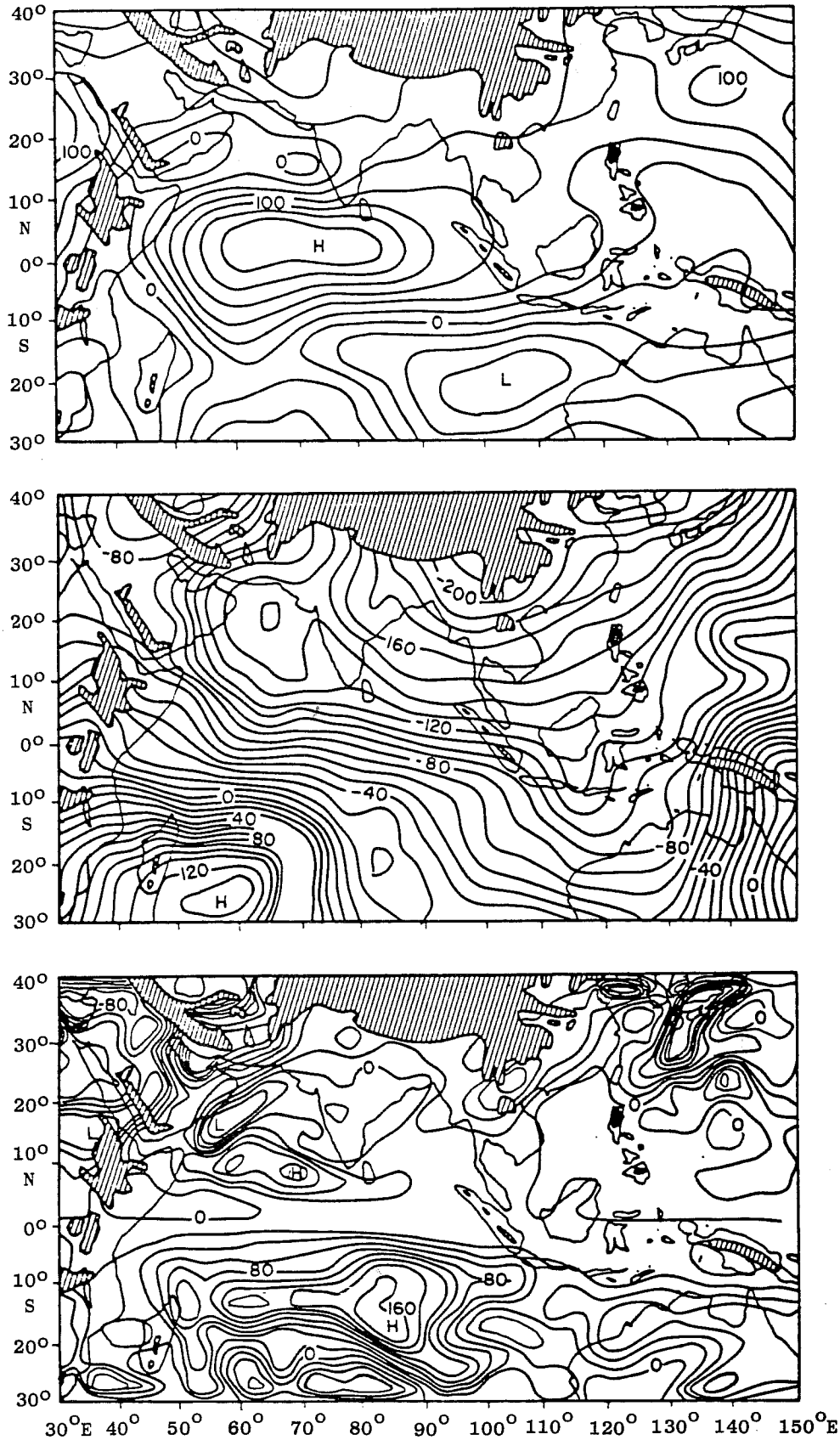

Fig. 5c As Fig. 5a but for onset.

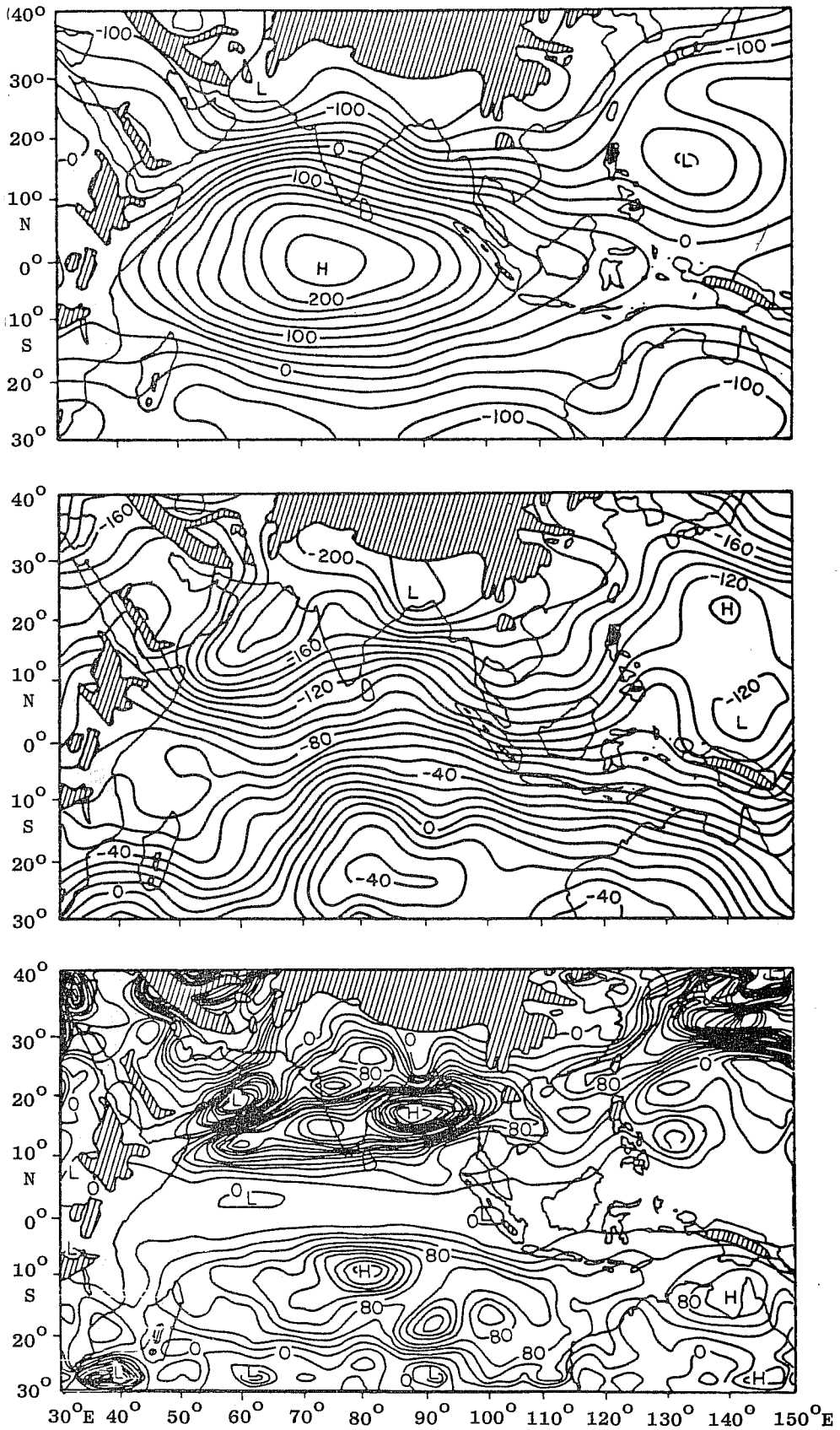

Fig. 5d As Fig. 5a but for active

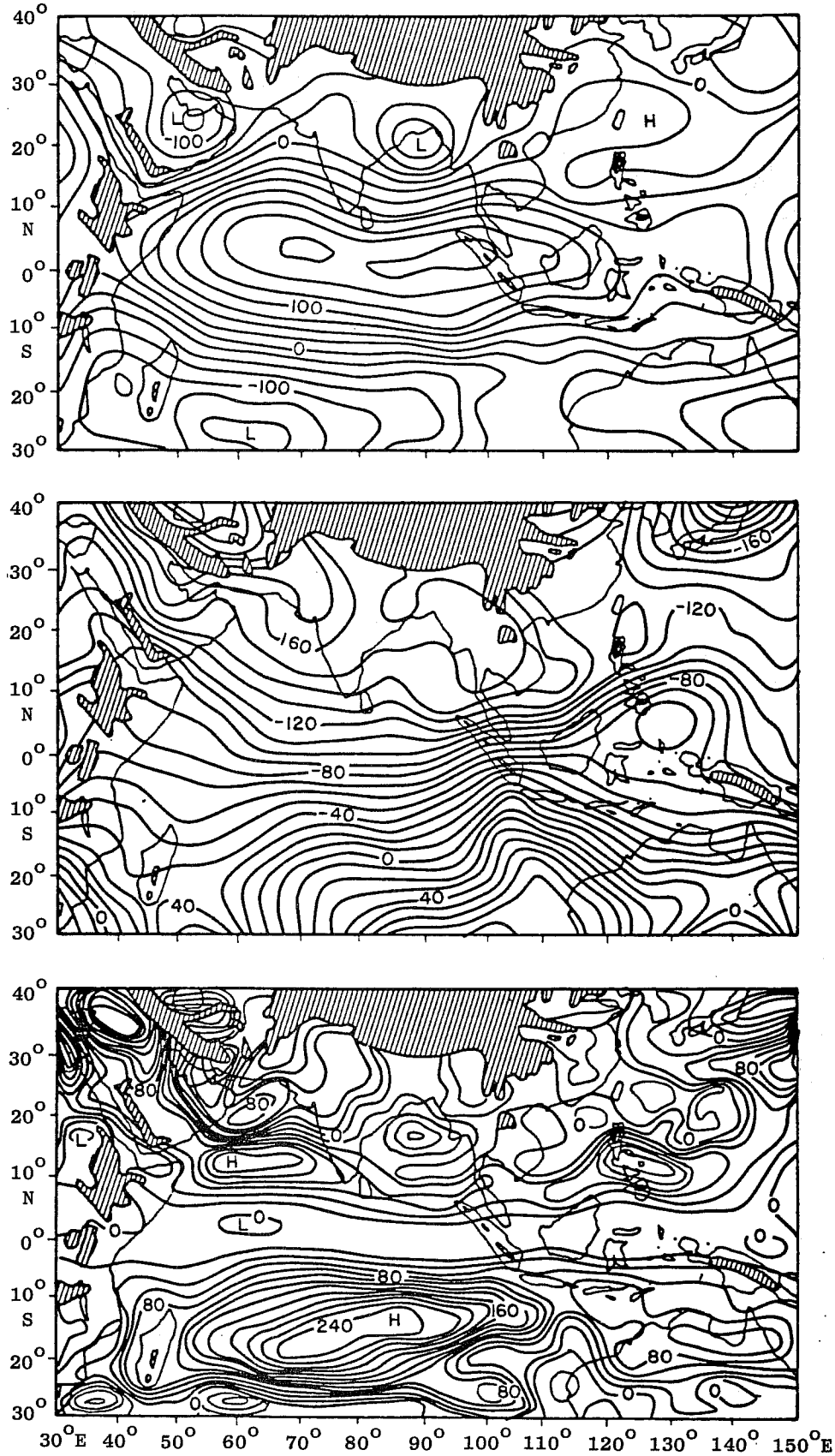

Fig. 5e As Fig. 5a but for monsoon depression over the North Bay.

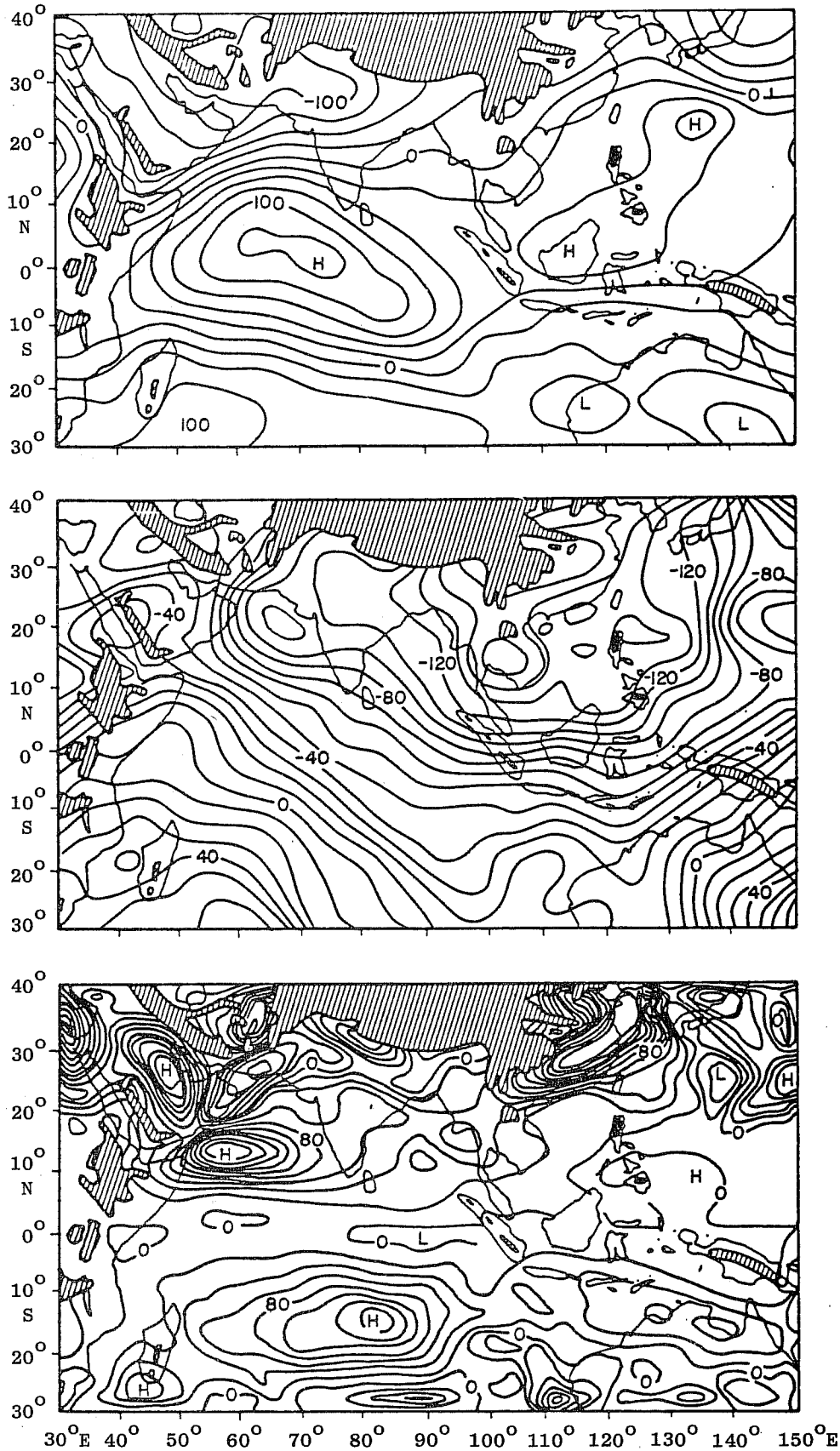

Fig. 5f As Fig. 5a but for break in monsoons.

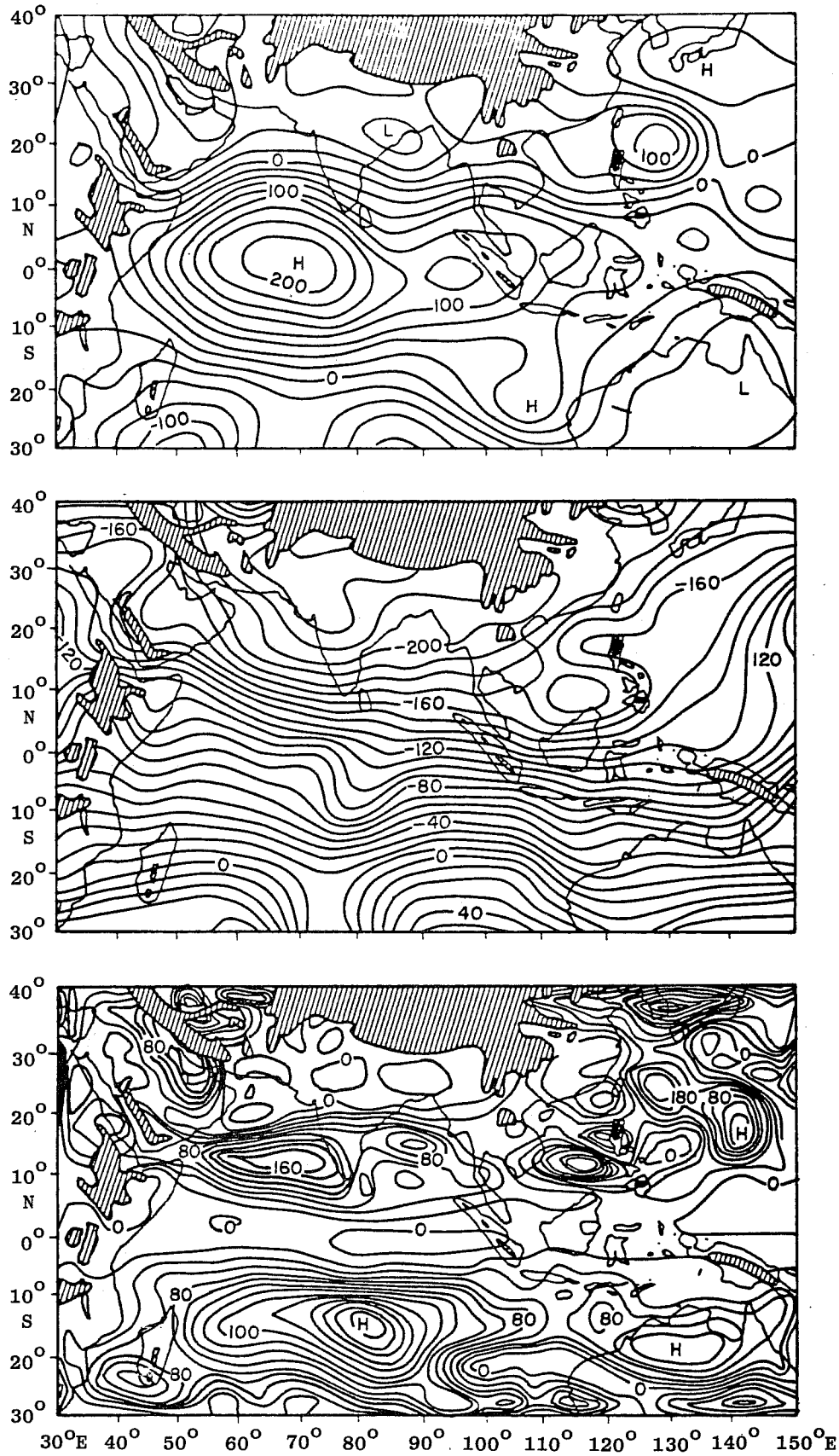

30°E 40° 50° 60° 70° 80° 90° 100° 110° 120° 130° 140° 150°E

Fig. 5g As Fig. 5a but for revival of monsoons.

In the context of those interactions the monsoon depression is also of considerable interest over the northern Bay of Bengal. A large region of $f\ \nabla\psi\cdot\nabla\chi > 0$ evolves during the period July 3 to 7 1979. Vector orientations suggest strongly that the development of the strong winds associated with this depression were evidently related to the evolution of $\nabla\psi$, $\nabla\chi$ vectors in this region. This suggests that the phenomenon may not be entirely barotropic.

Among the remaining terms of the $\langle\psi\cdot\chi\rangle$ interactions the term $\overline{\overline{\nabla^2\psi}\ \overline{\nabla\psi\cdot\nabla\chi}}$ has a negative sign for the most part within the computational domain. The sign is related to the fact that the monsoonal current within this domain has a negative relative vorticity. The magnitude of this term is of the order of $-200\text{x}10^{-6}\ m^2\ s^{-3}$ and is not able to counteract the effect of the leading term described above. The other remaining terms $\overline{\overline{\nabla^2\chi}\ (\nabla\psi\cdot\nabla\psi/2)}$ and $\overline{\overline{\omega J(\psi,(\partial\chi/\partial p)}}$ both exhibit a very sharp increase in early June and complement the first term $\overline{\overline{f\ \nabla\psi\cdot\nabla\chi}}$. However, the magnitudes of these terms lie around $+200\text{x}10^{-6}\ m^2\ s^{-3}$ and $+100\text{x}10^{-6}\ m^2\ s^{-3}$. We shall not go into a detailed map analysis of these terms here.

In summary we find that important fluctuations in the magnitudes of $\langle\psi\cdot\chi\rangle$ interactions occur due to the orientation of the vectors $\nabla\psi$ and $\nabla\chi$ and they are largely governed by the fluctuations in the orientation of the χ field. We believe that this provides the most important link between the differential heating and the establishment of strong monsoon westerlies and their fluctuations.

6. OBSERVED FIELDS OF DIFFERENTIAL HEATING

In order to portray simple fields of differential heating during the evolution of monsoons, we shall present estimates of vertically integrated net heating. These are constructed by a mix of methods.

i) Heating by condensation, $\overline{H}_c\ (x,y,t)$, is obtained by a calibration of the satellite brightness fields against available raingauge data sets. This was carried out separately using the continental and Island stations. The entire range of satellite brightness was first subdivided into a large number of subintervals. The daily brightness T_B values were next interpolated to the locations of the raingauge data sets. A large scatter of values of raingauge data were found for each of the subintervals of the T_B values. The large scatter of observed rainfall rates within the subintervals were next averaged, thus for each brightness temperature interval between T_B and $T_B + \Delta T_B$ a mean value of the raingauge rainfall was obtained. Fig.(6) illustrates an example

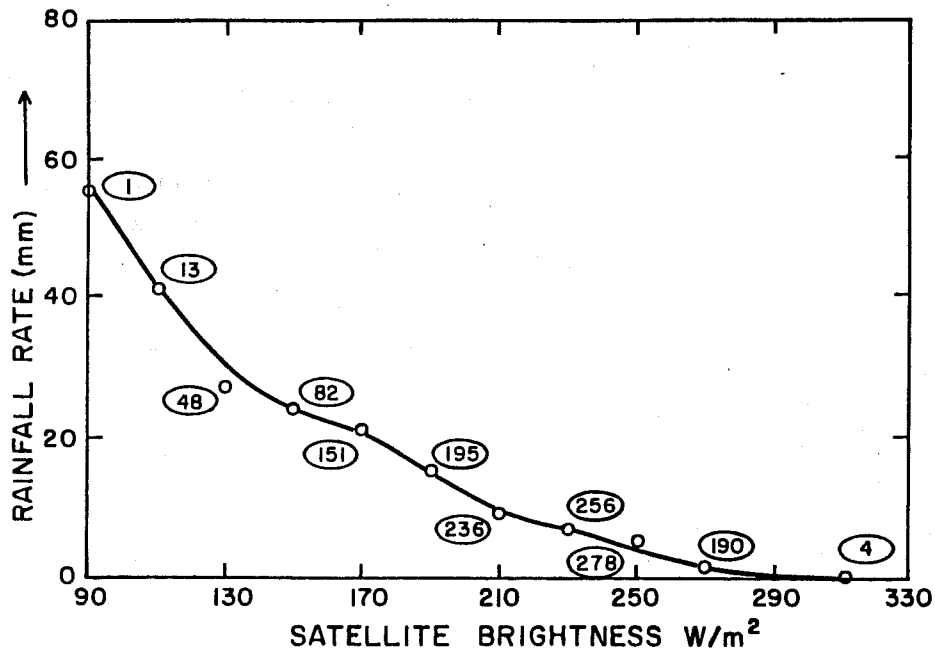

Fig. 6 Calibration of averaged raingauge rainfall data against the satellite IR brightness. The numbers along the curve denote number of observations.

of this curve over the Indian subcontinent. These curves were used as 'nomograms' for the construction of grid point values of rainfall rates from the fields T_B. The rainfall rates were next converted to heating rates and expressed in the units of deg C/day. Fig.(7) illustrates some examples of the heating rates obtained in this manner. In general the net vertically integrated rainfall heating are of the order of 6^{o}C/day. As we shall see later this is the largest among the various types of heating and contributes the most to the orientation of the differential heating between land and ocean.

ii) Heating by radiative processes, $\bar{H}_R(x,y,t)$. The calculations of short and longwave radiative processes were carried out using FGGE/MONEX observations and numerical algorithms used in our numerical weather prediction models, (Chang, 1980). Here, given the grid point values of large scale temperature, humidity, surface pressure, surface albedo and a ground wetness parameter the calculations determine the

i) shortwave irradiances via use of an absorptivity function
ii) longwave irradiances via use of the emissivity method, and
iii) surface heat balance, this includes a determination of surface temperature over land areas and corresponding fluxes of sensible and latent heat are determined.

The calculations of radiative transfer include a specification of clouds via use of relative humidity criterion. Cloud albedo and cloud absorptivity prorate the incoming shortwave irradiances and cloud surfaces also act as black body radiation for the longwave calculations. Low, medium and high clouds are permitted in these calculations. Some tests of these algorithms have been made against direct measurements of radiation provided by research aircraft during MONEX. The few tests show that the emissivity method is in close agreement with the observed measures, however, some discrepancies of the order of 0.5^{o}C/day were evident in the shortwave calculations. We feel that this is not very serious for the present exercise where vertically integrated values are largely determined by the longwave contributions which were much higher in magnitude. Fig.(8) illustrates a typical vertical profile of radiative heating calculated by this procedure. Typical values of cooling are of the order of 3 to 6^{o}C/day while the shortwave warming rates are around 0.5 to 1^{o}C/day.

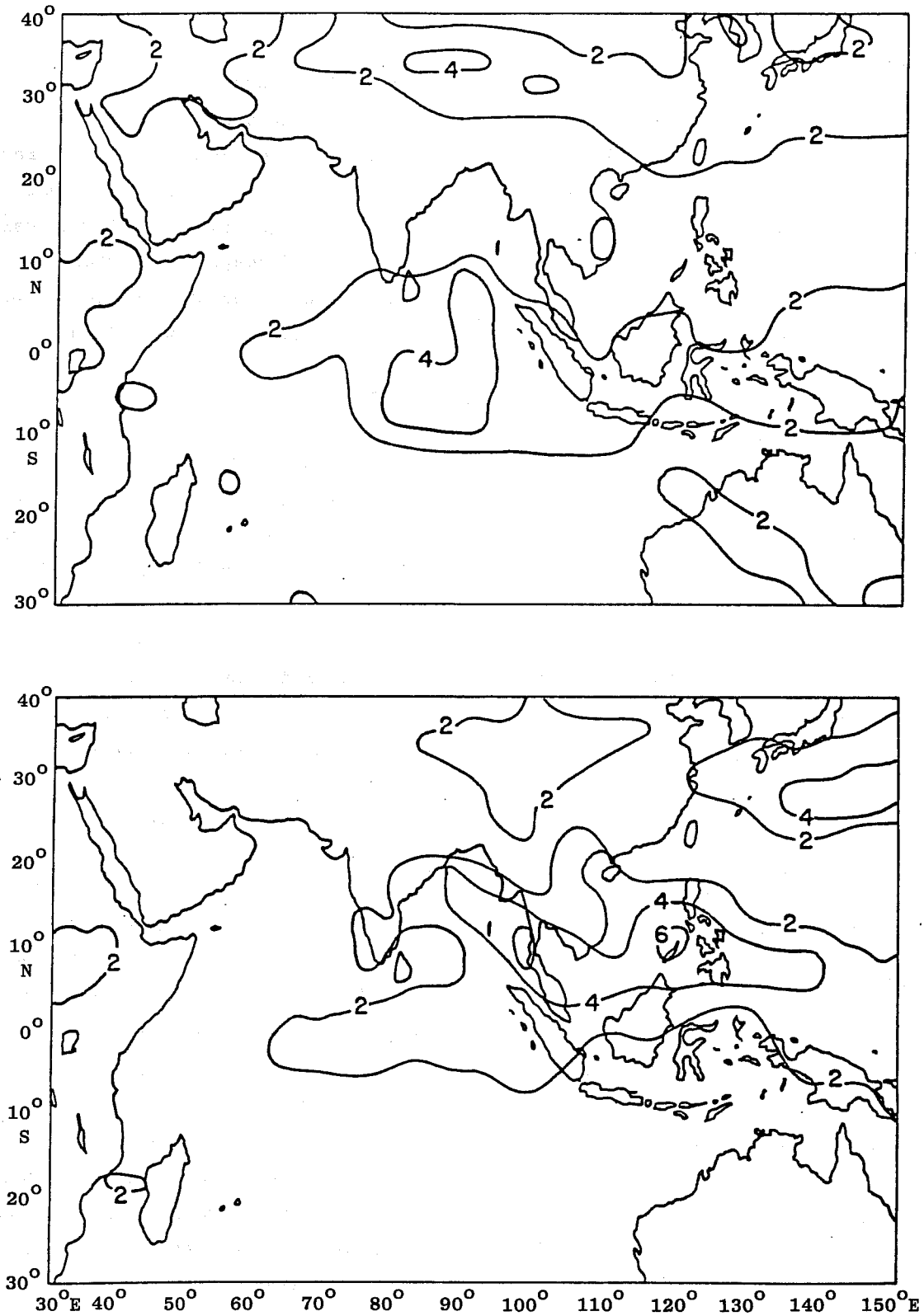

Fig. 7 a (top) b (bottom). Heating rate $\overline{Hc}$ in °C/day computed from rainfall estimates.

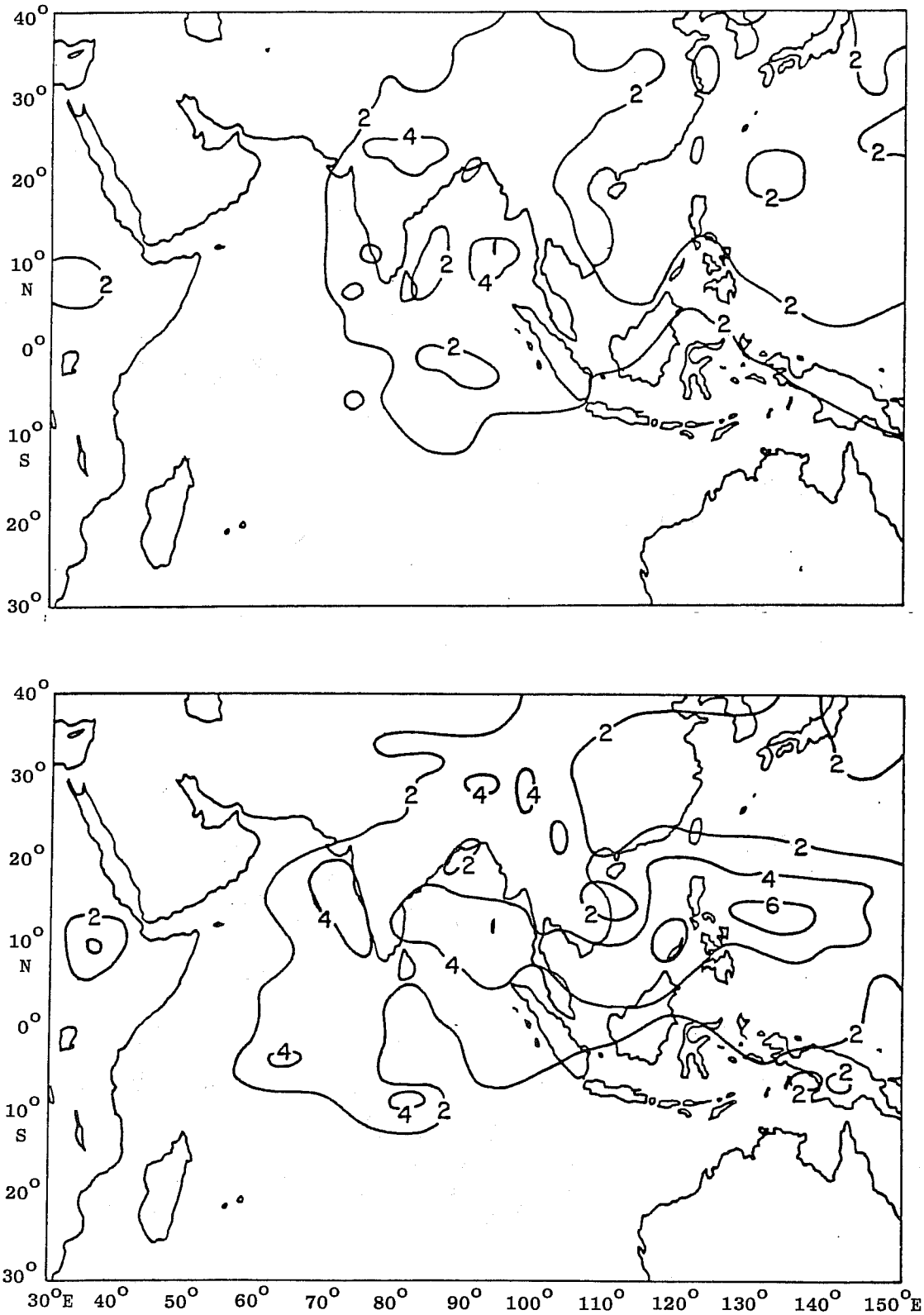

Fig. 7 c (top) d (bottom). As Fig. 7a,b.

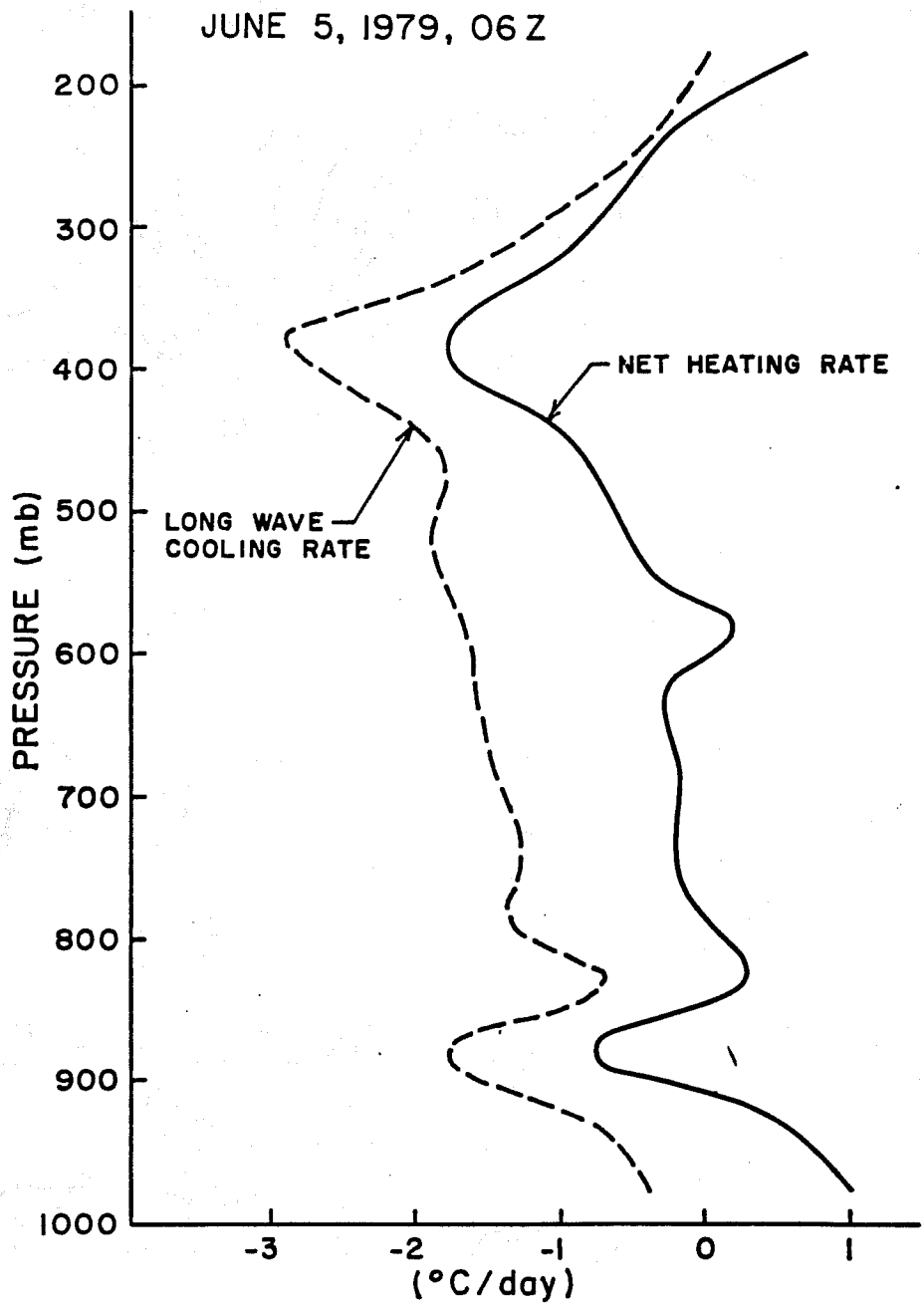

Fig. 8 Vertical profile of radiative heating rate for a typical sounding over the Arabian sea. Units ^{o}C/day.

iii) Surface fluxes of heat: The sensible heat flux contributes to the vertical integration of net heating while the latent heat flux (or evaporative flux) does not since the latter must first undergo a phase change and is thus included in (i). Since the Bowen ratio is very small, i.e. $\simeq 0.01$ in the tropics, the flux of sensible heat is quite small over the oceans being of the order of a few Watts/m^2. The land values of sensible heat flux, on the other hand are quite large, i.e. around 30 Watts/m^2 during a 24 hour period. This term was calculated in considerable detail, (a) over oceans using FGGE/MONEX marine data collections and bulk aerodynamics, i.e.

$$F_s = C_p \rho_o C_H V_o (T_w - T_a)$$

where V_o is the wind speed in m/s

T_w is the water temperature, ^oC,

T_a is the air temperature at the anemometer level ^oC.

ρ_o is the density of air at the sea level.

The exchange coefficient C_H was assigned a value 1.6×10^{-3} (nondimensional) following GATE studies. The units of F_S were expressed in Watts/m^2;
(b) over land areas the estimates of the flux of sensible heat are evaluated within the surface radiative heat balance calculations. The net tropospheric heating by this component comes from a vertical integral of $g\frac{\partial F_s}{\partial p}$ and is also expressed in the same final units, i.e. ^oC/day. The total heating is expressed by

$$\bar{H} = \bar{H}_C + \bar{H}_R + \bar{H}_S$$

Maps of $\bar{H}(x,y)$ for selected periods from the preonset, onset and the postonset phases of MONEX are illustrated in Figs. (9 a, b and c).

The preonset distribution of the period May 2 - 6, 1979, illustrates large net heating ($\simeq 4^oC$/day) south of the Indian continent over the Indian Ocean and large cooling of the order of 1.5^oC/day over the desert heat lows. The deserts over Saudi Arabia and northwestern India and Pakistan experience a net radiative cooling in spite of strong low level heating over the lowest kilometer. The deserts do not provide a differential heating $\nabla\bar{H}$ directed towards the heat lows from the oceans. On the contrary, the vertically integrated differential heating $\nabla\bar{H}$ points towards the direction of large convective rainfall regions. Blake et al (1981) have confirmed the presence of large scale descending motions over the heat lows from MONEX data sets. Only at the very low levels the differential heating vector $\nabla\bar{H}$ is directed towards the heat low, thus its role seems to be more thermally indirect (i.e. in the net warmer descending) in its contribution to the generation of eddy available potential energy. Synoptic experience suggests that the heat lows over

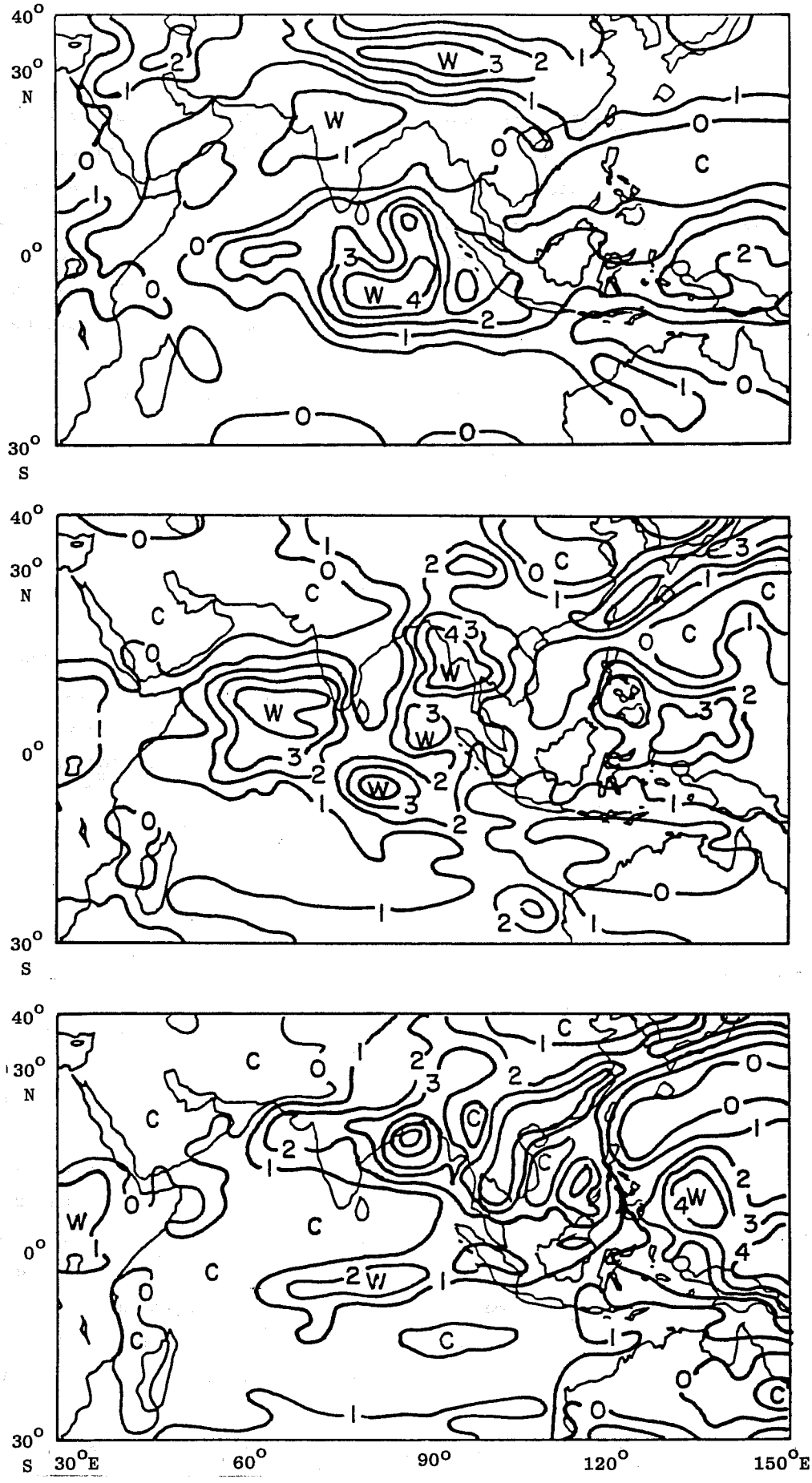

Fig. 9a,b,c. Charts of total heating $\bar{H}$ (°C/day) during pre-onset, onset and post-onset periods.

Arabia and India act to limit the northward penetration of moist air of the Indian Ocean. The separation line between the dry and the moist air has a zonal orientation and slopes equatorward with height and provides an easterly thermal wind and is associated with the weakening of the Somali jet.

The immediate preonset period, June 10-13, 1979, is characterised by the commencement of rains over northeast India and Burma (usually in the form of preonset thunderstorms). During this period heating rates of the order of $5^{o}C$/day were noted. Over the Arabian Sea the Somali jet had commenced to increase its speed by the 13th (see Fig.1). On its cyclonic shear side convection was the primary contributor to heating rates of the order of $3^{o}C$/day. As we shall see later the response of divergent circulation does not simply depend on the areal extent of convection. The region of strong heating near $90^{o}E$ had a very local divergent circulation and the Arabian Sea convection at this time did not exhibit a large scale inflow-outflow pattern over the deep troposphere. However, the dynamically active heating component at this period seemed to be that over northeastern India and Burma which had planetary scale vertical overturnings associated with it. A postonset differential heating is shown in Fig. (9c). This shows that heating rates of the order of $9^{o}C$ are found over the northern Bay of Bengal. Heating rates are very widespread over the land areas and the differential heating $\nabla\bar{H}$ is directed from the western Arabian Sea towards the northern Bay of Bengal. We shall not show detailed charts of the product $\overline{H'T'}$ (where prime is a departure from the zonal mean). However, the following comments on these fields are relevant here. The warm tropospheric air is found just north of the area of near equatorial convection during the preonset period. However, as one moves towards the onset and the postonset active period the axis of the deep tropospheric warmest air approaches the area of largest heating, as the latter moves northwards. Thus the heating begins to become more and more effective in generating eddy available potential energy. Its transformation to the divergent circulations via the covariance $\overline{\omega'T'}$ also shows a similar behaviour since the upward vertical motion field moves in close harmony with the field of large heating.

Sensitivity of the onset to the field of differential heating

The premise here is that an immediate preonset initial state is sensitive to the orientation of the prevailing large scale field of differential heating $\nabla\bar{H}$. The initial state provides the geometry of the large scale nondivergent flow component ψ ; the orientation of the differential heating determines the evolution of the divergent circulations χ; and under proper orientation of ψ and χ the $\psi \cdot \chi$ interactions become very effective in generating the kinetic energy of nondivergent motions leading to an onset. In order to formally test this idea a series of

experiments were carried out with a high resolution multi-level primitive equation model. In all these cases, essentially "the same initial state" was used, i.e. we selected a one week period June 5 to 11, 1979 (this is a week just prior to the dynamical onset). The motion, temperature, pressure and humidity variables were analysed and the average state Q(x,y,p) was obtained for the grid points between 1000 and 100 mb. See Fig. (10) for the vertical discretization of the model. At this point the irrotational and nondivergent parts of the motion field were evaluated at all levels and the irrotational part of this initial state was replaced by those from three periods respresenting late spring, preonset and post-onset periods. The moisture field for these three periods also replaced the weekly average of the above initial state. Thus the three initial states differ in their prescription of initial moisture and mass convergence. This provides a different field of differential heating at initial time for the three experiments since the heating is largely described by convection and in our model a modified Kuo's scheme (1974) determines convective heating as a function of the large scale moisture convergence. The three initial states do not appear all that different since the kinetic energy of the nondivergent component is much larger than that of the irrotational component. What is now common among the three initial states are the (i) nondivergent part of the motion, (ii) temperature and (iii) the geopotential (as the pressure) field. The heating field, as well as all other fields, are time dependent and evolve as the primitive equation model prediction evolves. The net differential heating is for the most part related to disturbances that move relatively slowly in four days. Thus the three experiments preserve, somewhat, the identity and the orientation of differential heating which was imposed initially.

The Florida State University's multi-level grid point primitive equation model is described in Krishnamurti et al (1975), Kanamitsu (1975) and Krishnamurti et al (1979). It includes the following features:

i) Semi-Lagrangian advection for the nonlinear advective terms;
ii) Euler backward time differencing scheme;
iii) Smoothed mountain, slope $|\nabla h| \leq 5 \times 10^{-3}$;
iv) Cyclic domain in the zonal direction;
v) Meridional velocity V = 0 at the north-south boundaries;
vi) All other variables assigned their initial zonally averaged values at the north-south boundaries for all time.
vii) Air sea transfer momentum, heat and moisture defined via Bulk Aerodynamic formulae;
viii) Cumulus convection based on a modified Kuo's scheme 1974;
ix) Large scale condensation in saturated regions where dynamic ascent of absolute stable air is encountered;

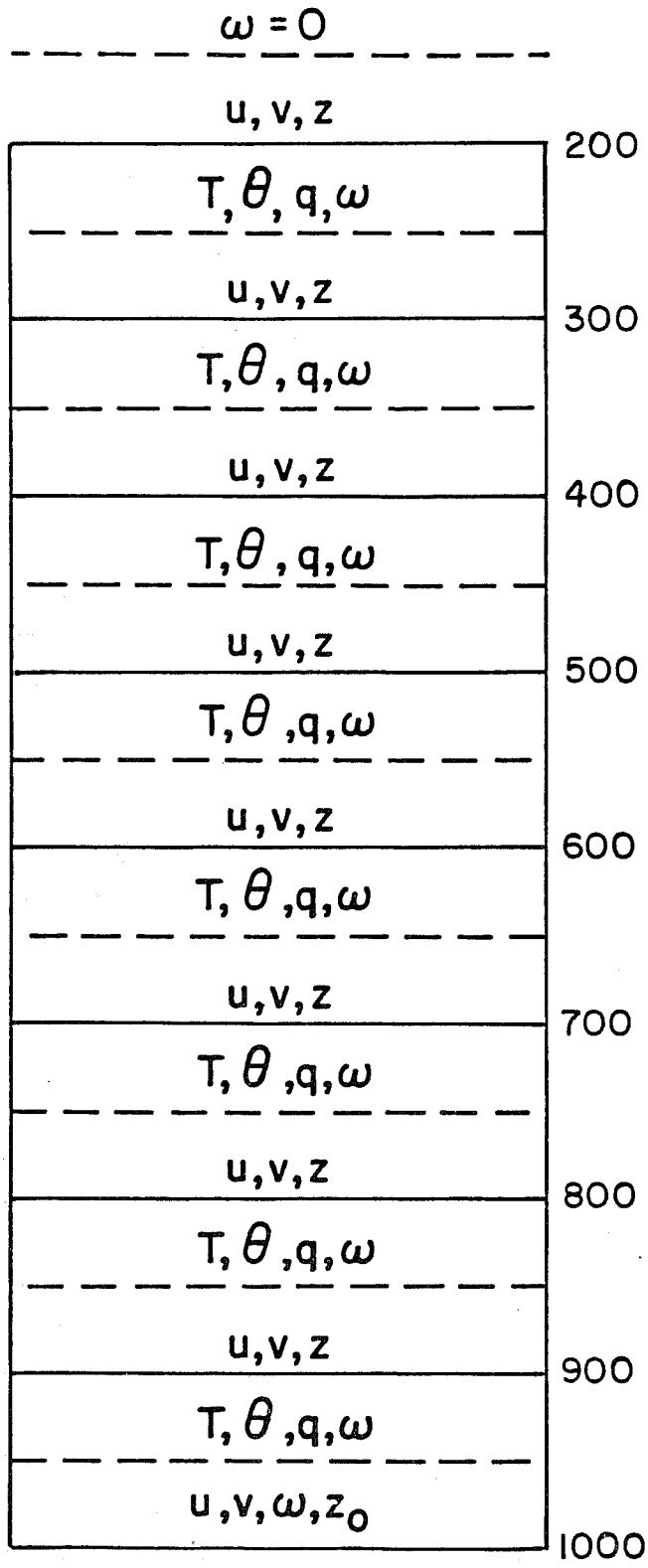

Fig. 10 Vertical descritization of the multilevel primitive equation model.

x) Short wave radiation based on an absorptivity function;

xi) Long wave radiation based on Emissivity Tabulations;

xii) Radiative calculations include a variable zenith angle and permits a diurnal change;

xiii) Radiative calculations include a specification of clouds based on relative humidity and cloud feed back is calculated following Chang (1980);

xiv) The surface heat balance over land areas determines the soil temperature, latent and sensible heat fluxes from the ground;

xv) Vertical velocity ω is assumed equal to zero at 100 mb and the mass-continuity equation is integrated downward to obtain ω at all other levels;

xvi) Initialisation: This is an important aspect of this study. In order to retain as much of the initial divergent circulations as were present initially, a static initialisation was first performed which merely adjusted the divergence at each level via a small correction term assuring its vertical integral to vanish. At this stage most of the observed wind (except for the divergence adjustment) is retained. The next stage is a forward-backward integration via dynamical initialisation. At the end of this initialisation most of the wind information is still retained - especially the divergent vertical circulations on the large scale. During the course of this initialisation some adjustment of mass and temperature does occur. Furthermore, the vertical motions implied by the initial wind produce adiabatic warming and cooling, which are not compensated by diabatic cooling or warming since all of the physical processes are suppressed in the dynamical initialisation. This produces some distortion of the pressure and the temperature field. This evidently is not very large since most of this is recovered in a short time during the actual forecast where the diabatic effects are reintroduced. For tropical initialisation this approach has the advantage that one can retain the large scale divergent circulation at the end of initialisation. However, that does not guarantee that this feature would be retained during the course of numerical prediction if the parameterisation of cumulus convection does not adequately describe the field of the differential heating.

We shall next describe an intercomparison of the results of the three sensitivity experiments.

Results of numerical integrations: The domain of integration extends from 30°E to 150°E, 30°S to 40°N, 100 to 1000 mb and uses a 2° mesh. The initial state is not shown here, suffice it is to state that, the flows describe an anticyclonic flow over the northern Arabian Sea with dry northerly flow over India. The Somali jet is absent at this time and deep westerlies are found south of 5°N. At the end of 96 hours the three experiments show marked differences in their

evolution. Figs. (11 a,b,c) show the 850 mb flow fields for the late spring, preonset and the postonset experiments. The structure of the cross equatorial flows is a measure of the evolution of the monsoons. The first two experiments do not show any evolutions of the typical monsoonal low level cross-equatorial flows. The third experiment exhibits a rapid evolution of the monsoons. Fig. (11 d) illustrates the well marked cross-equatorial flows at 72 hours after the initial time, the southerly flows continue on towards the region of the strong convective heating near the northern Bay of Bengal. It appears from these experiments that the evolution is quite sensitive to the initial fields of divergent circulations and the differential heating. This also points to the need for proper initialisation in numerical weather prediction to assure that they retain the features of the observed divergent circulations, since large errors can arise from the types of sensitivity shown here. Aside from the differences in the evolution of circulations the three experiments also exhibit interesting differences in the ψ - χ interactions, and in the energetics. In the following calculations are carried out for an inner domain identical to those for the observed fields.

Fig. (12 a,b and c) illustrates the predicted evolution of zonal kinetic energy, eddy kinetic energy and the conversion from the zonal to the eddy kinetic energy. In all of these diagrams the larger magnitudes for the postonset-differential-heating-experiment stand out. The conclusion that can be drawn for this is that the zonal flow evolves much more strongly for this experiment and the barotropic process acquires a significant strength under the proper orientation of differential heating. As we have stated earlier, most of total kinetic energy is in the non-divergent component and a large proportion of this must come from the irrotational component. Thus barotropic energy exchanges and barotropic instability may yet require that the $\langle \psi \cdot \chi \rangle$ interactions supply energy to the basic flows steadily. The evolutions of $\langle \psi \cdot \chi \rangle$ interactions for the three experiments are shown in Fig. (13). Here again the 'post-onset' evolution is quite distinct from the other experiments. Although the magnitudes of the $\langle \psi \cdot \chi \rangle$ interaction did not quite reach the levels of observed magnitudes ($\simeq$ 600 units as against 100 units for the experiment) at the end of 4 days the rapid growth for the third experiment is a convincing evidence of the sensitivity of the onset to the initially imposed field of differential heating.

It would be desirable to carry out further experiments along these lines with a bigger model to look at the planetary scale problem.

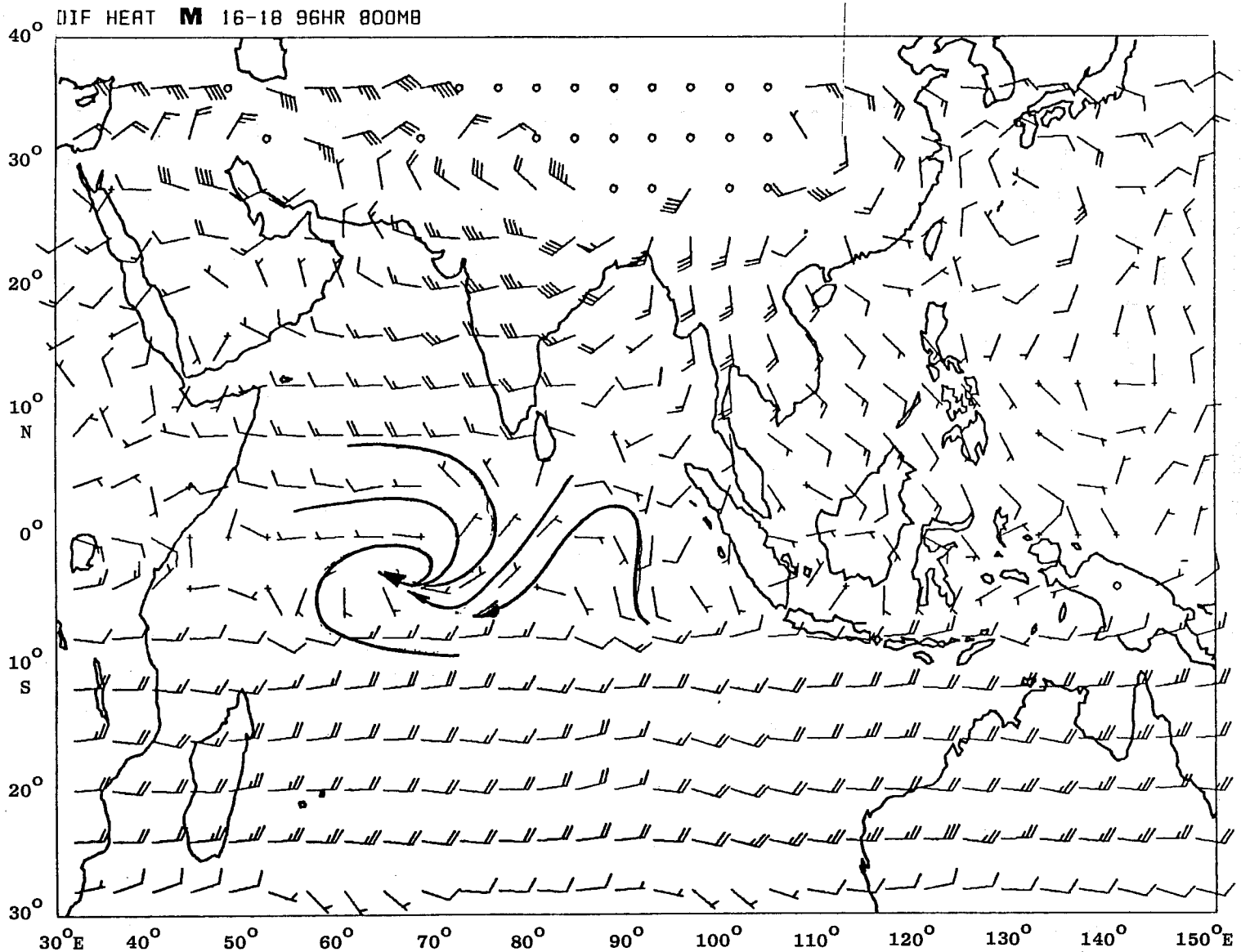

Fig. 11 Predicted 850 mb wind field for the three experiments. a) Late spring at 96 hours.

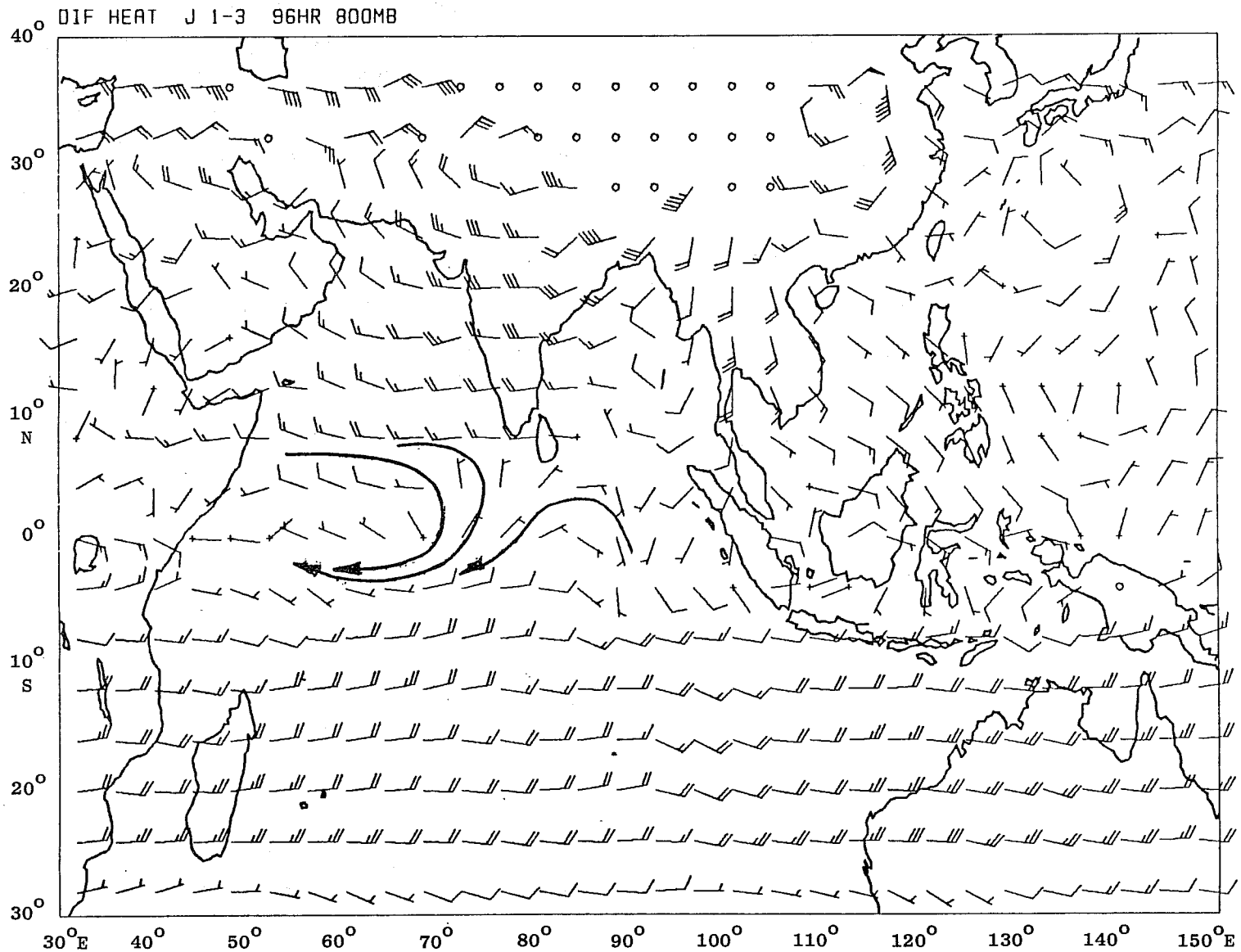

Fig. 11b As Fig. 11a but for pre-onset at 96 hours.

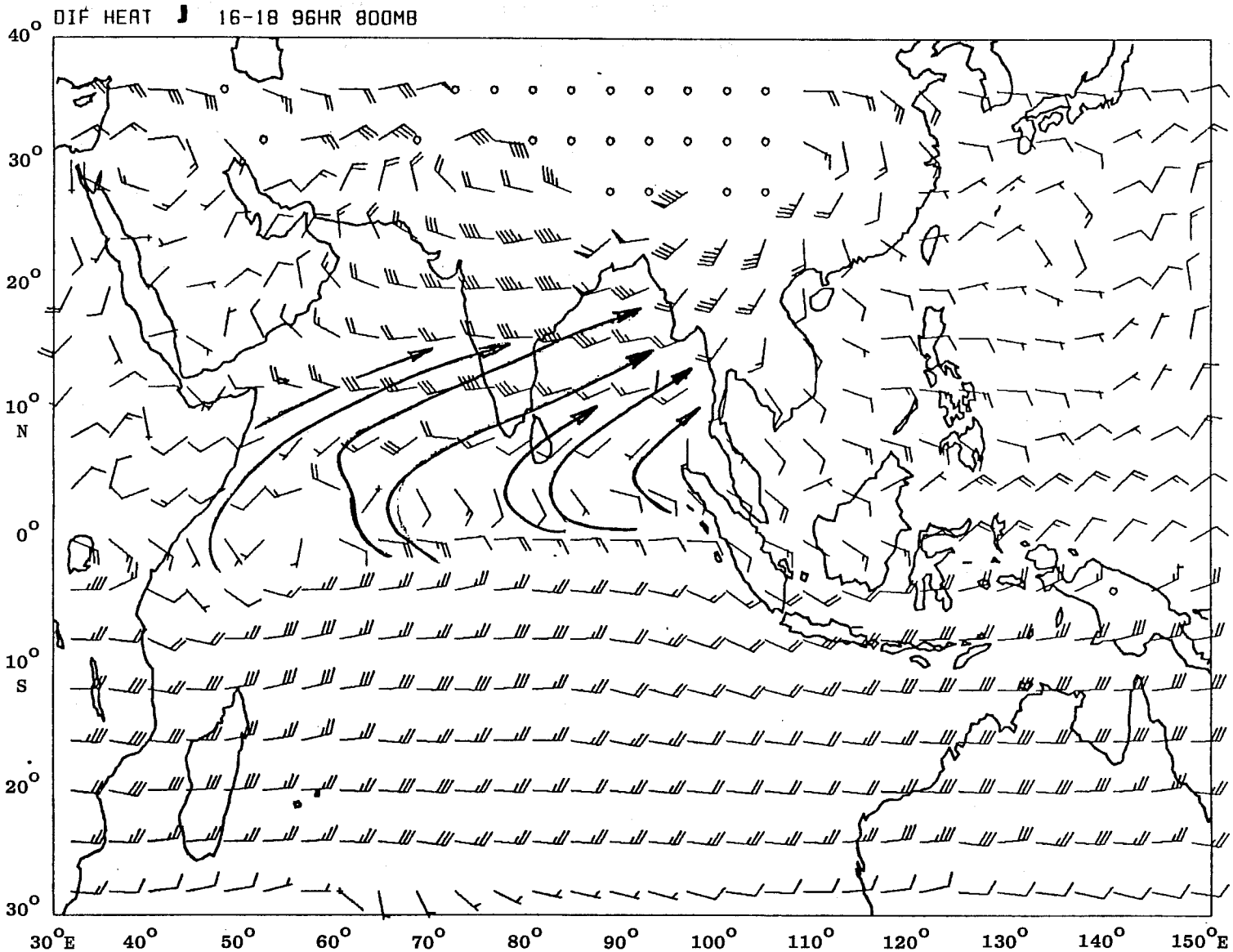

Fig. 11c As Fig. 11a but for post-onset at 96 hours.

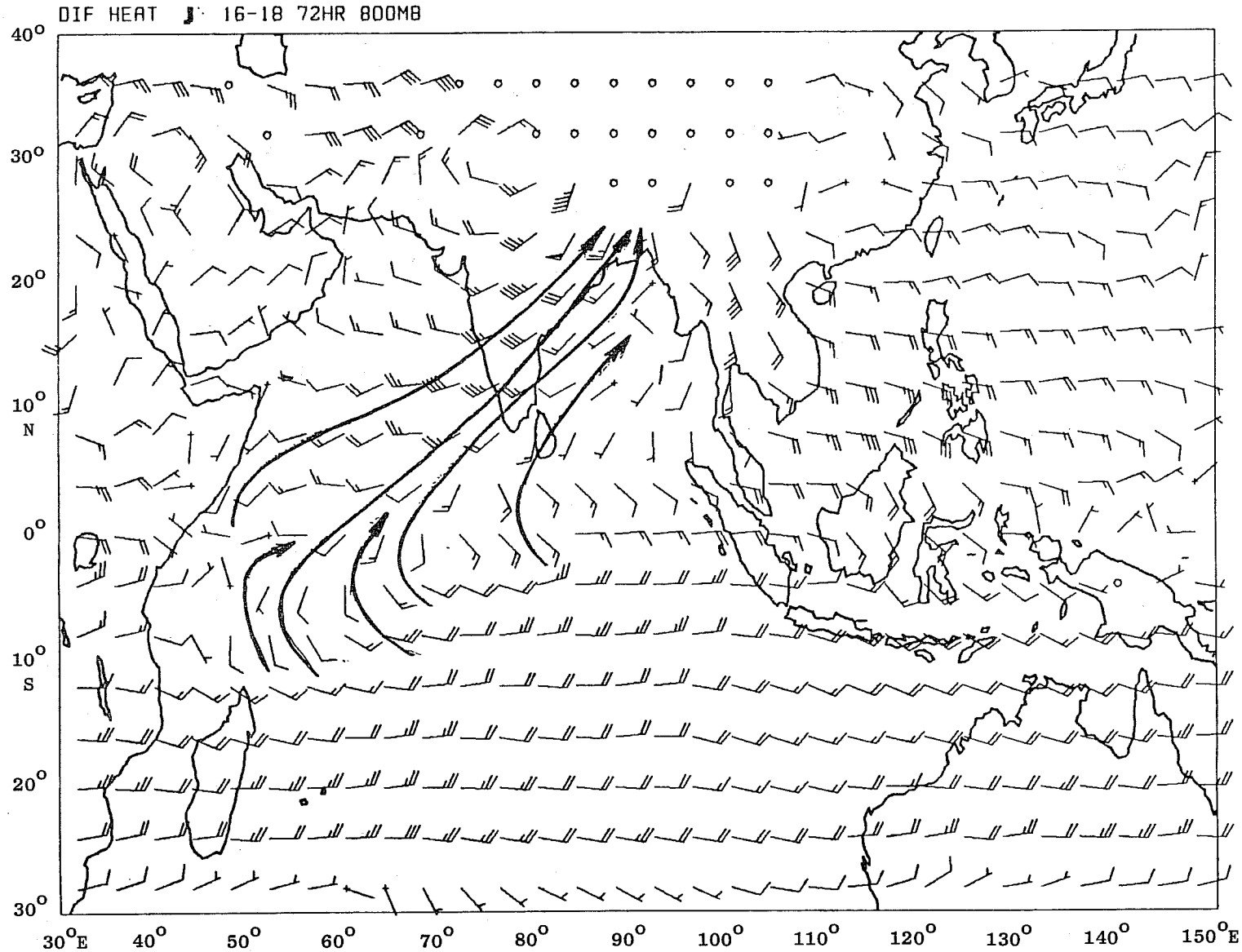

Fig. 11d As Fig. 11a but for post-onset at 72 hours.

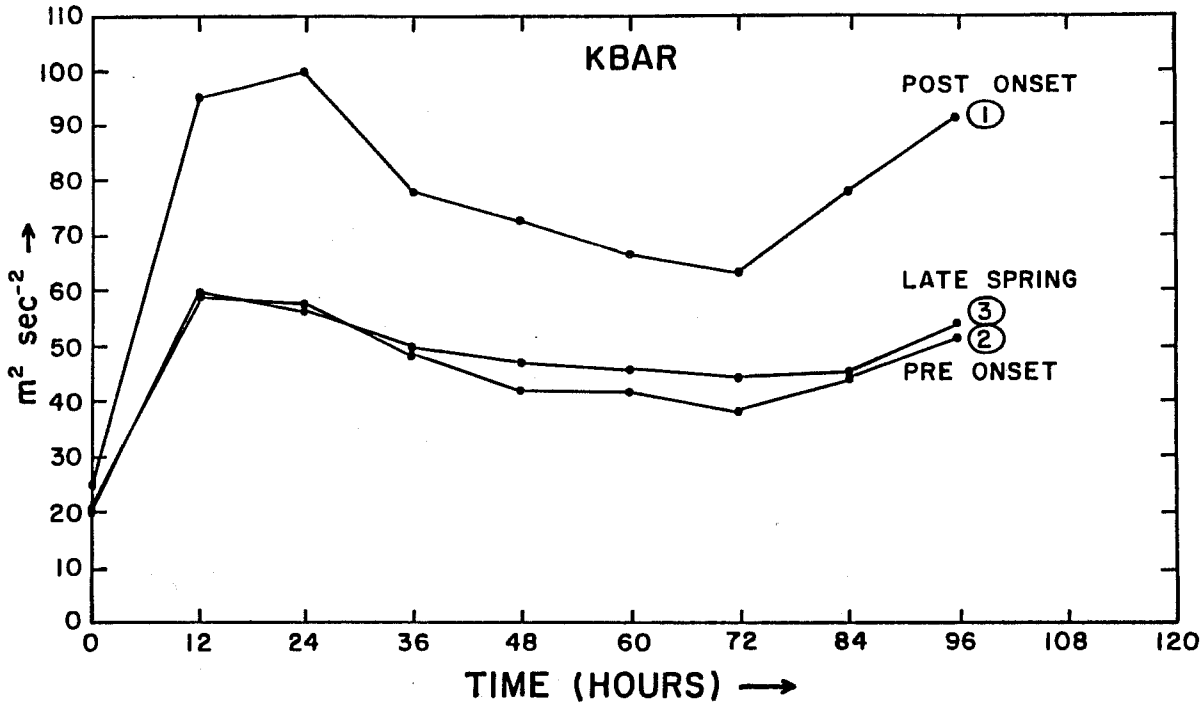

Fig. 12 Evolution of zonal kinetic energy $\bar{K}$, eddy kinetic energy K' and their conversion $\langle \bar{K} \cdot K' \rangle$ for the three experiments.

a) $\bar{K}$

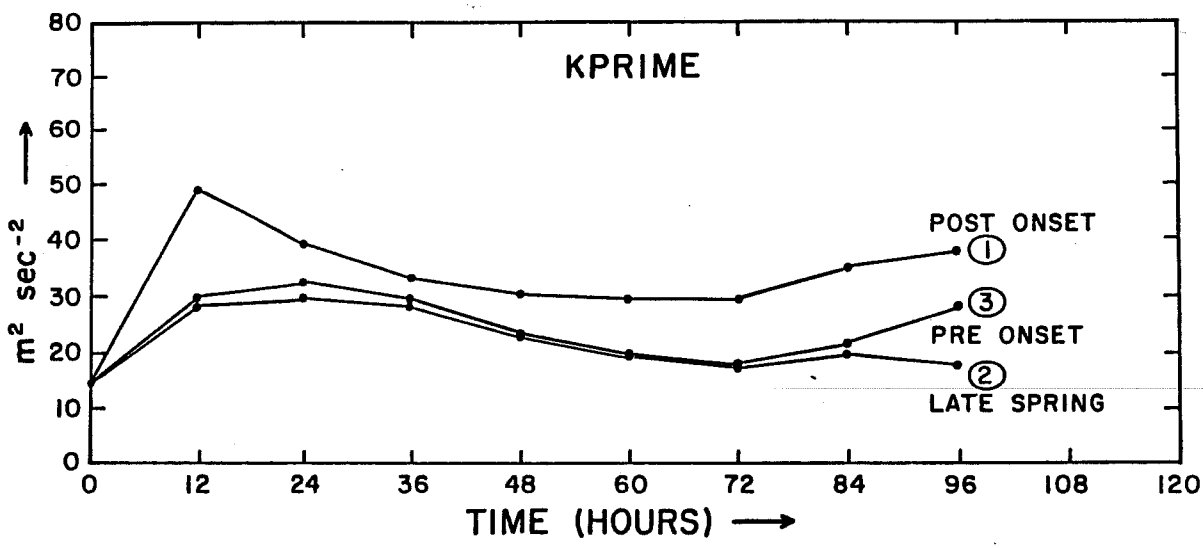

Fig. 12b As Fig. 12a but for K'.

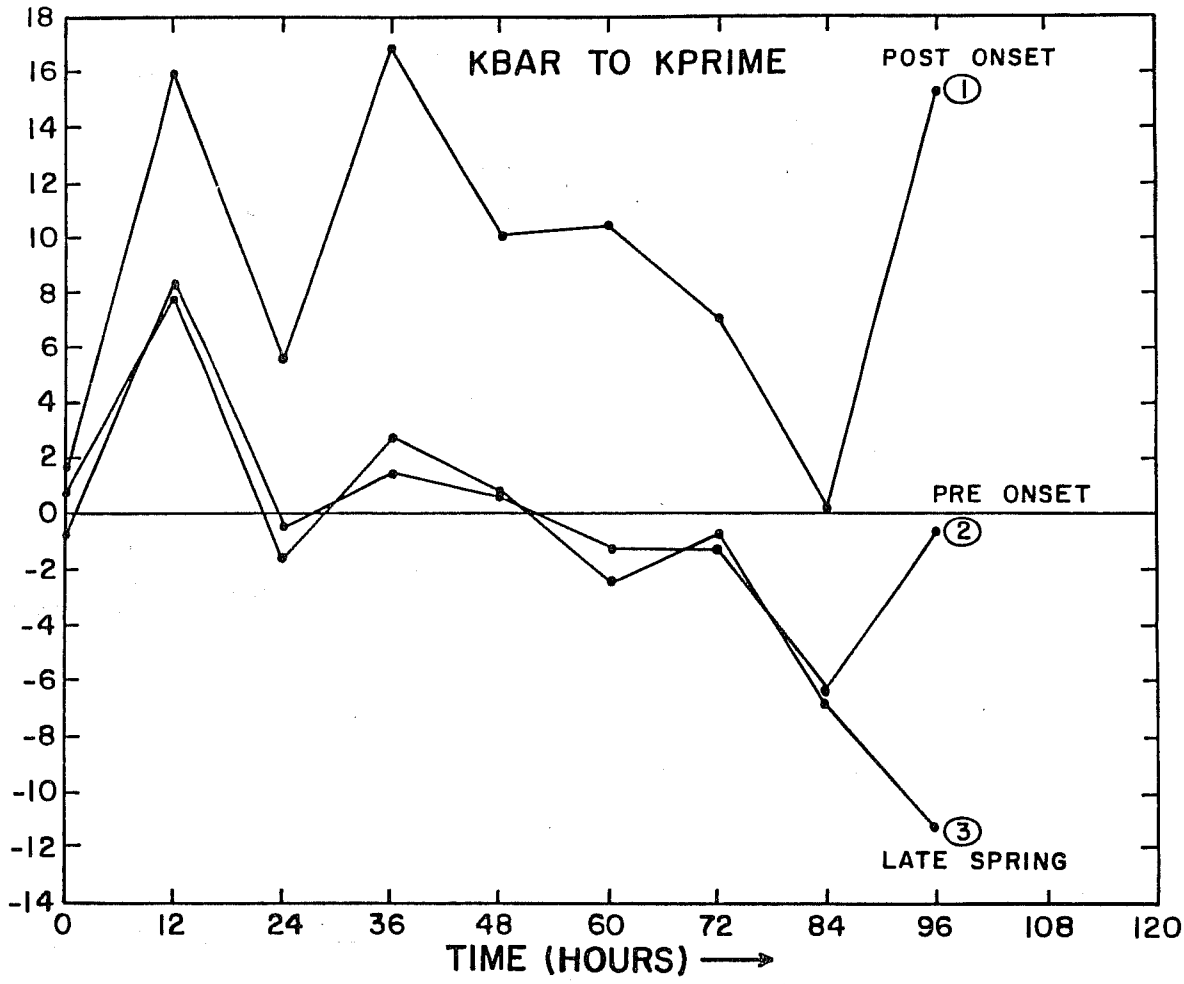

Fig. 12c As Fig. 12a but for $\langle \bar{K} \cdot K' \rangle$

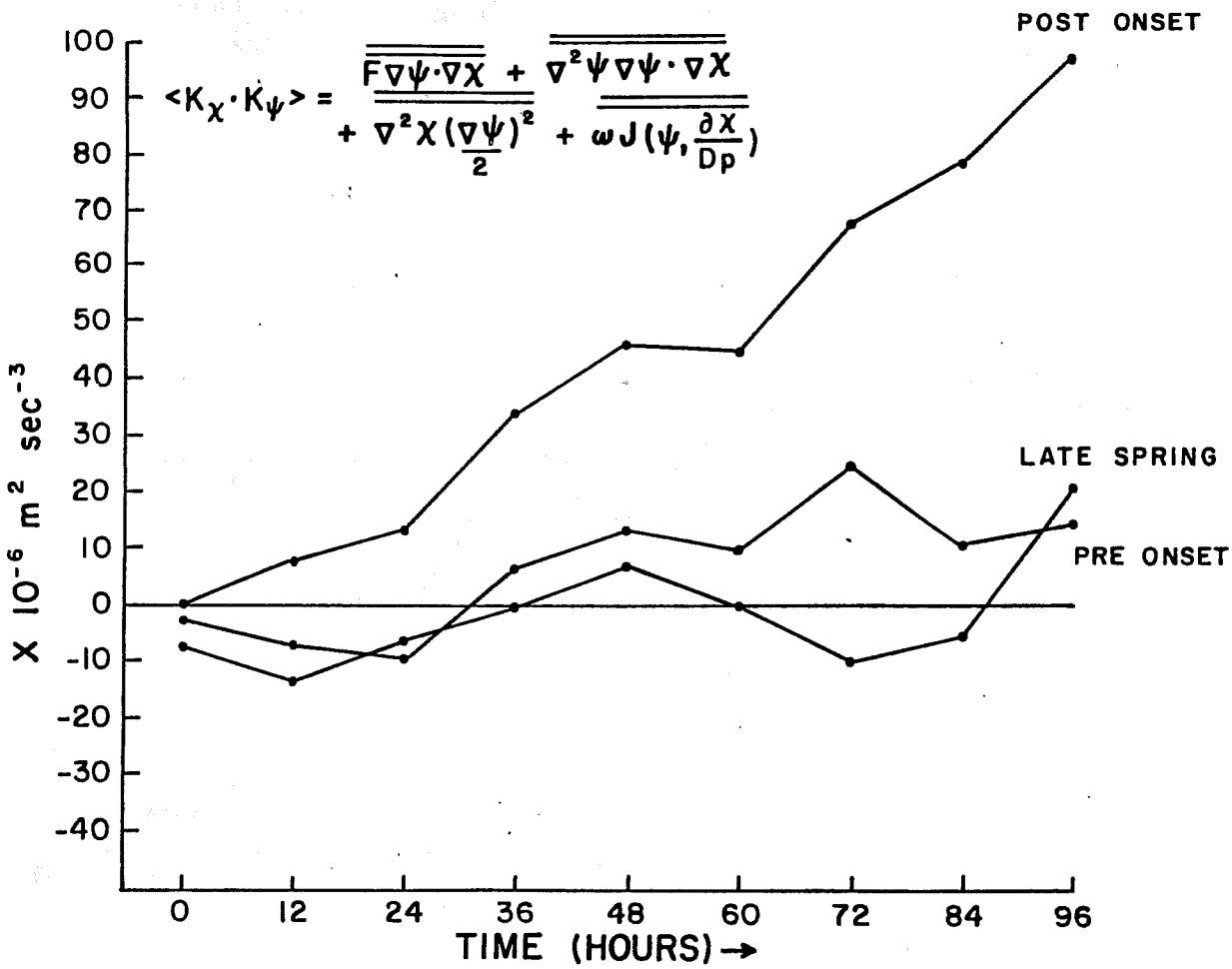

Fig. 13a The evolution of the energy exchange from the irrotational to the nondivergent component for the three experiments.

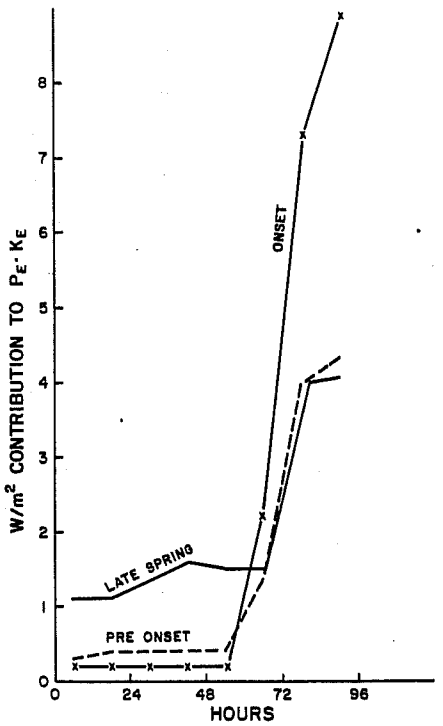

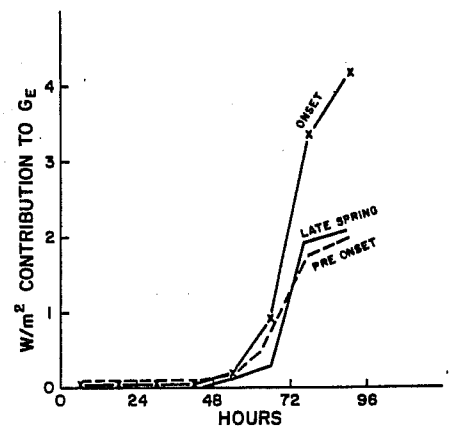

Fig. 13 b (top) c (bottom). As Fig. 3a.

CONCLUDING REMARKS

This study has emphasized the role of the energy exchanges from the irrotational to the non-divergent component in the evolution of the monsoons. This exchange is viewed as an important link among a sequence of processes that begin from the build up of the large scale field of differential heating from sea and land and leading eventually to the strengthening of the monsoonal westerlies and it supplying energy to the eddy motions via the barotropic processes.

Among the sequence of events we identify:

i) Storms with deep convection proceed northward and north-westward over Indochina and Burma around the late part of May and early June. Around this time premonsoon thunderstorms occur over northeastern India. This sequence of synoptic events leads to an evolution of the field of differential heating $\nabla\bar{H}$ between land and sea. A gradual evolution of the field of $\nabla\bar{H}$ can be noted with reversal in its orientation.

ii) As the heating moves northwards the generation and the release of eddy available potential energy increases.

iii) This leads to a build up of divergent circulation whose centres follow the deep convection regions identified in (i) above. The orientation of the geometry of divergent circulation is closely linked to the orientation of the differential heating.

iv) When the divergent overturnings are more meridonal (rather than zonal) over the Arabian Sea a favourable setting for the exchange of energy from the irrotational to the nondivergent circulation is found. This seems to be related to the fact that the nondivergent flows over the Arabian Sea remain more nearly zonal while the irrotational flows fluctuate in their orientation.

v) The periodic changes in the orientation of the irrotational vector field leads to a periodic strengthening and weakening of the monsoonal flows.

vi) Zonal flow accelerations lead to eddy motion and a number of barotropically unstable vortices, e.g. onset vortex, monsoon depression are noted to occur during periods of the strengthening of zonal flows.

Finally, a numerical experiment was designed to test the aforementioned ideas on the sensitivity of the monsoon onset to initial fields of differential heating. This experiment showed a rapid increase of zonal and eddy kinetic energy only when a post-onset field of differential heating was used. The diagnosis of the experiment also exhibited a rapid increase of the energy exchange from the irrotational to the nondivergent component.

ACKNOWLEDGEMENTS

This material is based upon work supported jointly by the National Science Foundation and the National Oceanic and Atmospheric Administration under Grant Number ATM-7819363.

REFERENCES

Blake, D., J. Fein, T.N. Krishnamurti, and S. Low-nam, 1981: The heat low over Saudi Arabia during MONEX. To be published by WMO.

Chang, Chia-bo, 1980: On the influences of solar radiation and diurnal variation of surface temperatures on African distrubances. Ph.D. dissertation submitted to the Department of Meteorology of the Florida State University. p. 1-152.

Daley, R., C. Girard and J. Henderson, 1976 : Short term forecasting with a multilevel spectral primitive equation model. Atmosphere, 14, 98-134

Eliassen, E.M., B. Machenhauer and E. Rasmussen, 1970: On a numerical method for integration of the hydrodynamical equations with a spectral representation of the horizontal fields. Rept. No.2, Institute of Theoretical Meteorology, University of Copenhagen.

Kanamitsu, M., 1975: On numerical prediction over a global tropical belt. Dept. of Meteorology, Florida State University, Rept. No. 75-1, 282 pp.

Krishnamurti, T.N., M. Kanamitsu, R. Godbole, C.B. Chang, F. Carr and J. Chow, 1976: A study of a monsoon depression II: Dynamic structure. J. Met. Soc. Japan, 54, 208-225

_____, H.L. Pan, C.B. Chang, J. Ploshay, D. Walker and A.W. Oodally, 1979: Numerical weather prediction for GATE. Q.J. Roy. Met. Soc., 105, 979-1010.

_____, P. Ardanuy, Y. Ramanathan and R. Pasch, 1981: On the onset vortex of the summer monsoons. Mon. Wea. Rev., 109 344-363

Kuo, H.L., 1974: Further studies of the parameterization of the influence of cumulus convection on large-scale flow. J. Atmos. Sci., 31, 1232-1240.

Ramanathan, Y., 1981: A short range numerical prediction experiment on the onset of monsoons. FSI REport No.81-1, Department of Meteorology, Florida State University, Tallahassee, Florida 32306, U.S.A. pp.1-25.